COLLÈGE DE FRANCE
—1530—

Chaire de Physique de la Matière Condensée
Antoine Georges

Réseaux de Neurones, Apprentissage et Physique Quantique

Cours 6:

Réseaux de neurones et fonctionnelle de densité pour la structure électronique

Cycle 2022-2023
6 juin 2023

Image Credit: Javier Robledo-Moreno

Machine Learning and Neural Networks for Quantum Physics

Lecture 6

Neural Networks and Density Functional Theory

Applications to Electronic Structure

Image Credit: Javier Robledo-Moreno

Seminar (11h30):
Ambroise van Roekeghem
Université Grenoble-Alpes, CEA-LITEN

Machine learning force fields for materials science

Ambroise van Roekeghem
Université Grenoble Alpes, CEA, LITEN

The use of machine learning techniques to build force fields matching ab initio data at a fraction of the computational cost has exploded in the last decade. In this seminar, I will first introduce the atomic descriptors typically used by such force fields. I will illustrate their advantages by discussing some recent applications, but also some of their limitations or technical difficulties that may arise. Finally, I will discuss some of the current developments in the field.

Mailing List
(Weekly announcement of lecture and seminar, etc.)

Send email to: listes-diffusion.cdf@college-de-france.fr
Subject line: subscribe chaire-pmc.ipcdf
…or: unsubscribe chaire-pmc.ipcdf

You can also just send me an email to be placed on the list

Website:

https://www.college-de-france.fr/site/antoine-georges/index.htm

Lectures are video recorded
and available on the website

Today's menu:

- Cont'd from lecture 5: Hidden Fermion Determinantal States: some results and conclusion

- Fundamentals of Density Functional Theory in a nutshell

- Teaching a neural network to implement the Hohenberg-Kohn correspondence

- Constructing Density Functionals using Machine Learning

- Some Applications

- Disclaimer: this is only an incomplete overview of an emerging and burgeoning field... basically to make you want to read/learn more about it.

Hidden Fermion Determinantal States (HFDS)

Fermionic wave functions from neural-network constrained hidden states

Javier Robledo Moreno[a,b,1], Giuseppe Carleo[c,d], Antoine Georges[a,e,f,g], and James Stokes[a,h]
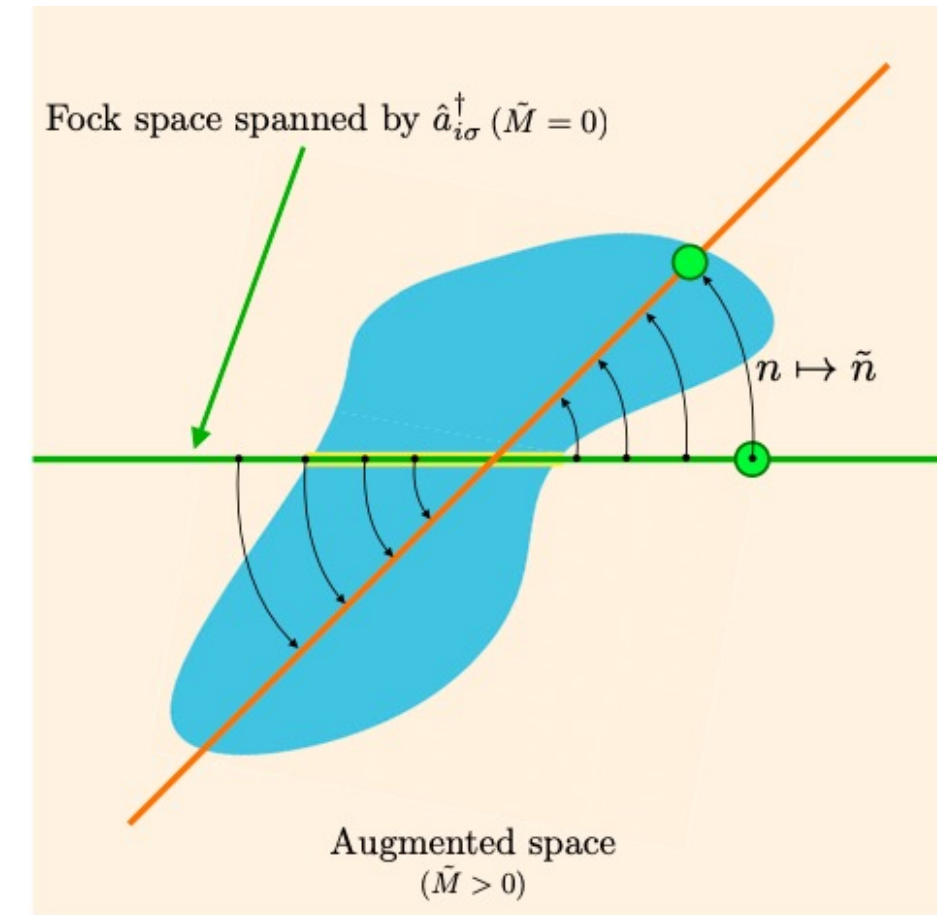
- For a recent extension to continuum space and application to nuclear matter, see: A.Lovato et al. Phys Rev Research 4, 043178 (2022)

HFDS: The Basic Concept

Fock space spanned by $\hat{a}_{i\sigma}^{\dagger}$ $(\tilde{M} = 0)$

$n \mapsto \tilde{n}$

Augmented space
$(\tilde{M} > 0)$

● Target correlated state

SDs in augmented space

SDs in physical space

HFDS enlarges the Hilbert space with *fermionic* `hidden' modes.

The wave function is a Slater determinant in the enlarged space, subject to a constraint for projecting it back to the physical space.

This results in a correlated/entangled wave-function

J. Robledo-Moreno et al.
PNAS, 2022

Fig. 1. Depiction of the geometrical interpretation of the hidden fermion formalism. The Fock space spanned by the visible-fermionic modes $\hat{a}_{i\sigma}^{\dagger}$ is represented by the green horizontal line. The augmented Fock space is represented by the light orange plane (plane of the paper). The orange diagonal line represents the subspace in the augmented Fock space that is isomorphic to the physical Hilbert space after applying the constraint function (black arrows). The collection of SDs in the augmented space is represented by the blue shape, and the intersection with the subspace of just visible DOFs is marked in yellow. This intersection corresponds to the physical Hartree–Fock states. The constraint function changes the collection of states that represent the physical Hilbert space bringing the target correlated state close to a Slater determinant in the enlarged space.

HFDS: The General Concept

$$\boxed{\begin{array}{l} |\Psi\rangle = \hat{P}_f\, \varphi_1^+ \cdots \varphi_N^+\, \chi_1^+ \cdots \chi_{\tilde{N}}^+\, |0\rangle \\[4pt] \hat{P}_f\, :\, ,\ \widetilde{n} = F(n)\ ,\ \tilde{x} = f(x) \end{array}}$$

$$\psi(x) = \det \begin{pmatrix} \phi_v(x) & \chi_v(x) \\ \phi_h[f(x)] & \chi_h[f(x)] \end{pmatrix}$$

These lines parametrized by neural networks

$$= \varepsilon_{\sigma(x)} \det\left[(n(x), F(n(x)) \star \Phi\right]$$

$$\Phi = \begin{pmatrix} \Phi_{p\alpha} & \Phi_{p\tilde{\alpha}} \\ \Phi_{\tilde{p}\alpha} & \Phi_{\tilde{p}\tilde{\alpha}} \end{pmatrix} = \begin{pmatrix} \phi_v & \chi_v \\ \phi_h & \chi_h \end{pmatrix}\ ,\ \dim = \begin{pmatrix} M \times N & M \times \tilde{N} \\ \tilde{M} \times N & \tilde{M} \times \tilde{N} \end{pmatrix}$$

$$\varphi_\alpha^+ = \sum_{p=1}^{M} c_p^+ \Phi_{p\alpha} + \sum_{\tilde{p}=1}^{\tilde{M}} h_{\tilde{p}}^+ \Phi_{\tilde{p}\alpha}$$

$$\chi_{\tilde{\alpha}}^+ = \sum_{p=1}^{M} c_p^+ \Phi_{p\tilde{\alpha}} + \sum_{\tilde{p}=1}^{\tilde{M}} h_{\tilde{p}}^+ \Phi_{\tilde{p}\tilde{\alpha}}$$
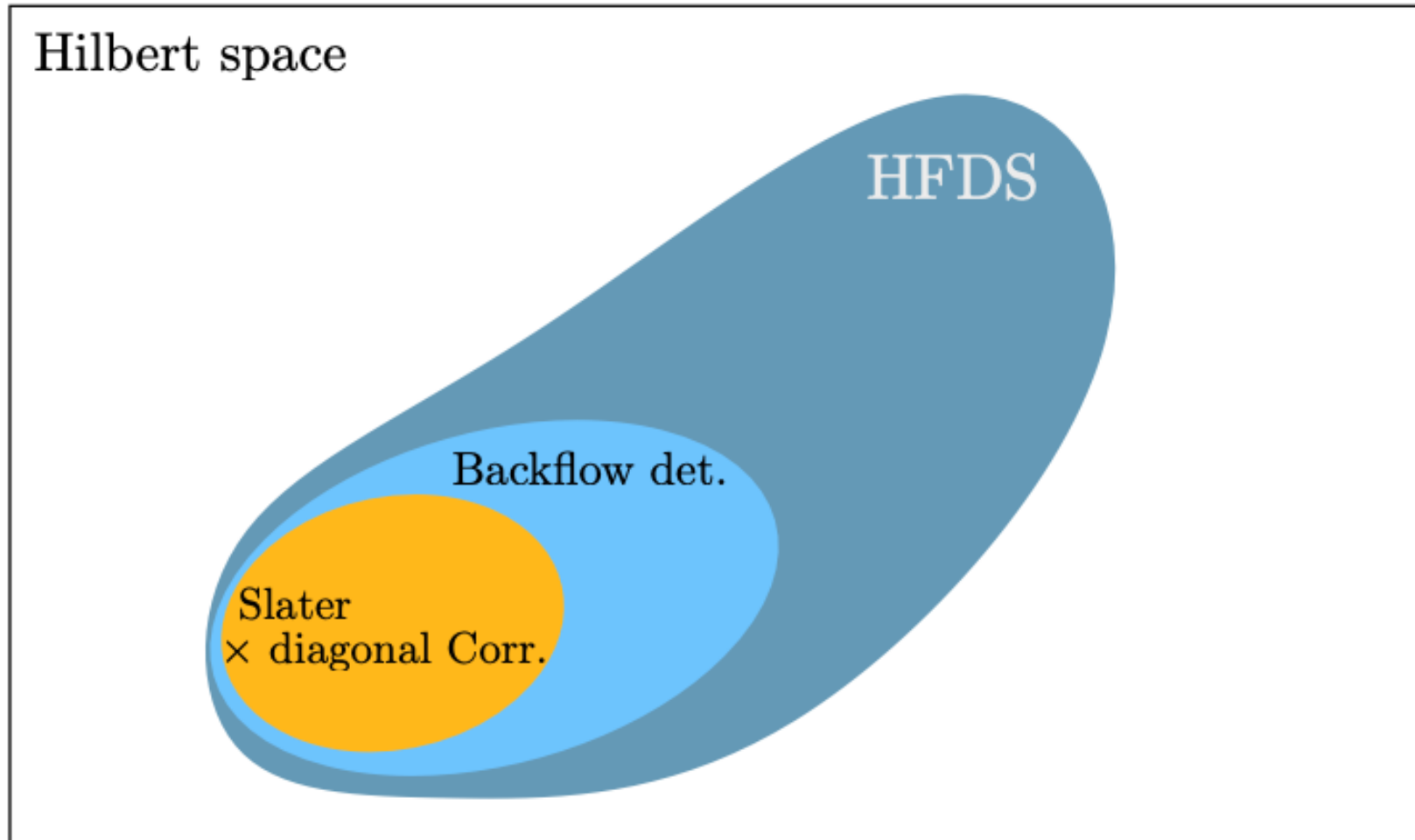
Figure 6.2: Venn diagram of the expressive power of classically tractable (amplitudes can be evaluated in polynomial time) determinant-based trial states, in the Hilbert space spanned by a finite number of basis elements (discrete degrees of freedom). HFDS stands for hidden fermion determinant state, in this case with $\tilde{N} = N$. Backflow det. stands for a single $N \times N$ backflow determinant. Slater $\times$ Corr. is the $N \times N$ Slater determinant multiplied by a diagonal correlation factor.

Figure courtesy Javier Robledo-Moreno
See J R-M's PhD thesis for more details

Parametrization of a Hidden Fermion Determinantal State by neural networks
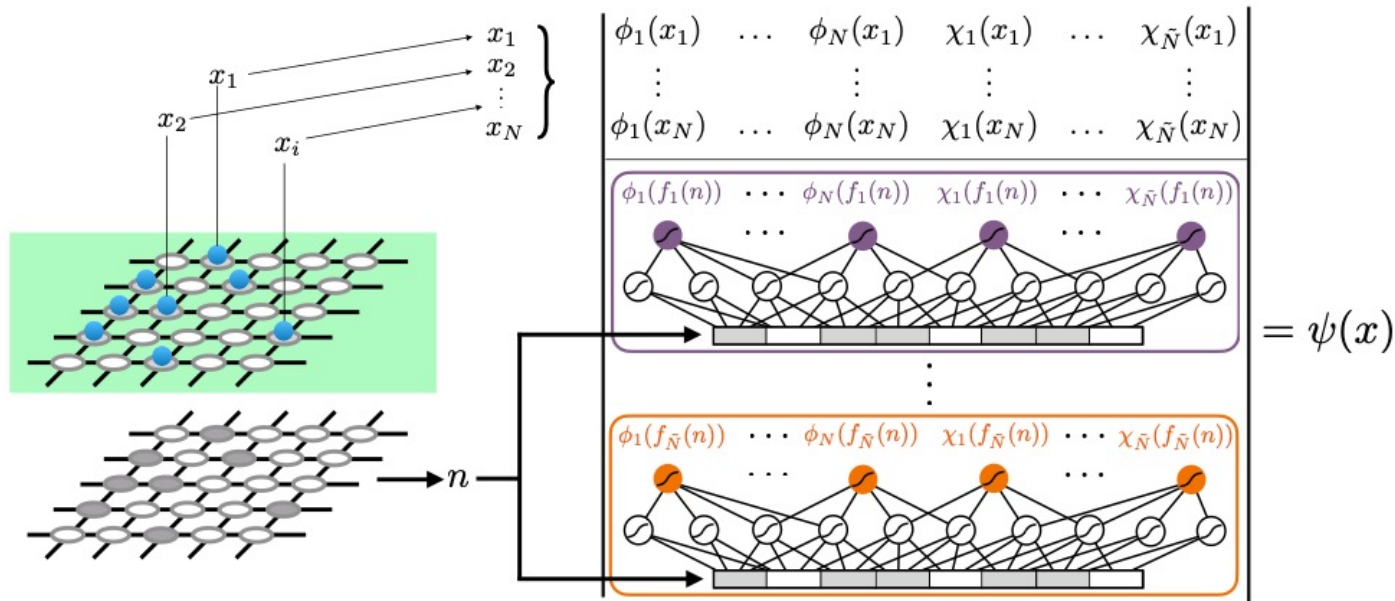
Each row of the hidden sector is parametrized by a different perceptron.
For example, with 2 layers:

$$[\phi_1^h[f_i(x)], \cdots, \chi_{\tilde{N}}^h[f_i(x)]] = \tanh\left(\tanh\left(\mathbf{n} \cdot \mathbf{w}_i^{(1)} + \mathbf{b}_i^{(1)}\right) \cdot \mathbf{w}_i^{(2)} + \mathbf{b}_i^{(2)}\right)$$

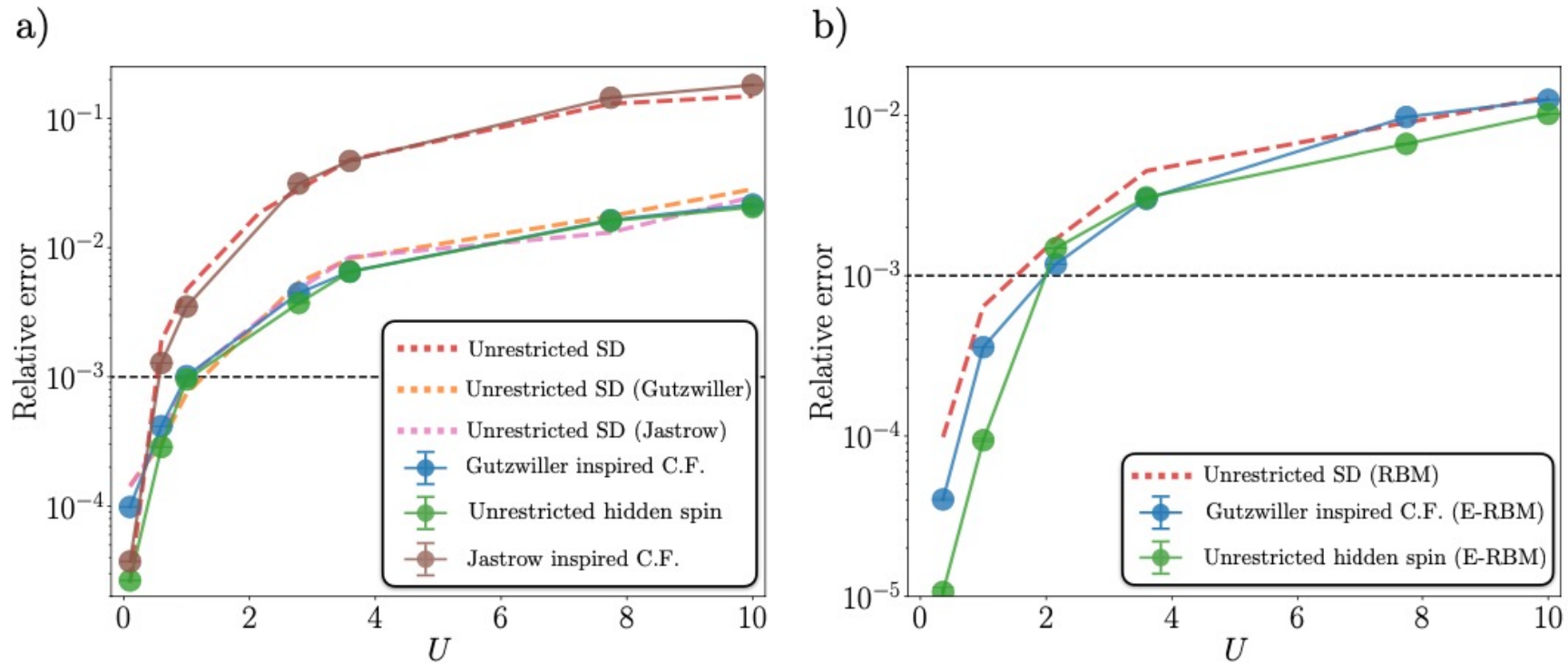# HFDS with physically motivated constraints: benchmark on 4*4 Hubbard model at ½-filling

Fig. 1. Benchmarks of physically motivated constraint functions with ED energies in the 4×4 Hubbard model at $n = 1/2$ average physical site occupation. Results from standard wave function *ansätze* are shown as dashed lines for comparison purposes. (a) Relative error in the ground-state energy as a function of the coupling constant U. The different constraint function *ansätze* are a single Slater determinant in the augmented Fock space with no projections. (b) Same as panel (a) including a complex RBM projection factor both in the control unrestricted HF *ansatz* and a E-RBM factor in the the hidden fermion *ansätze*.

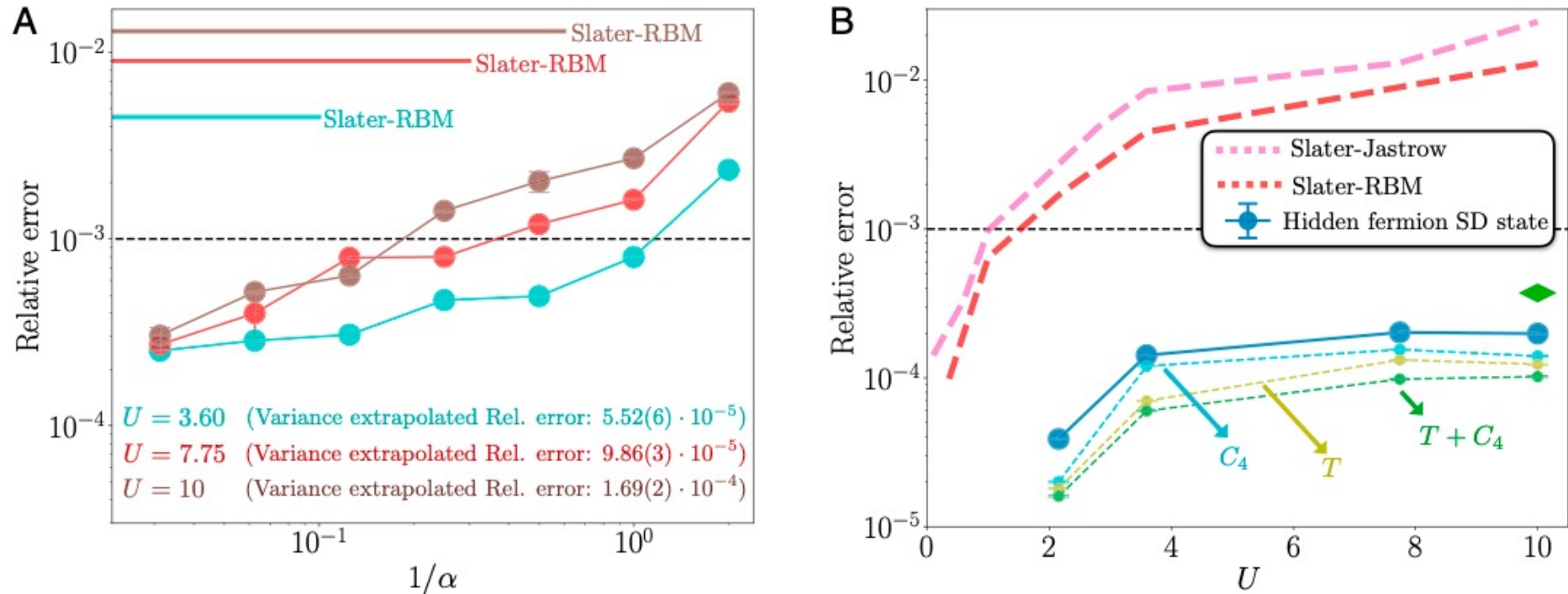# Numerical results with NN parametrization: 4*4 Hubbard model at ½-filling

Fig. 3. Exact diagonalization benchmarks of the ground-state energy in the 4×4 lattice with periodic boundary conditions. (A) Relative error in the ground-state energy as a function of the inverse of the width density α of the single-hidden-layer neural networks parameterizing the rows of the hidden submatrix. Average physical site occupation is $n = 1/2$ and $\tilde{N} = 8$. Different values of U are considered, as indicated by each color. The error for a Slater-RBM ansatz (main text) with hidden neuron density $\alpha = 32$, at the same values of U, is included for comparison. Indicated is also the relative error from the variance-extrapolated energy for each value of U (see *SI Appendix* for details). (B) Relative error in the ground-state energy as a function of the coupling constant U, at $n = 5/8$ average site occupancy (first closed shell) and $\tilde{N} = 10$. The rows of the hidden submatrix are given by single-hidden-layer neural networks with $\alpha = 64$. The errors from Slater–Jastrow and Slater-RBM ansätze are included for comparison. The green diamond is the relative error found with the state-of-the-art, tensor-network–based ansatz from ref. 46. Shown is also the relative error according to the projection of the converged hidden-fermion determinant state to the subspace of invariant wave functions under the action of $\pi/2$ rotations (C_4) and the group of all possible translations T with $K = 0$ momentum, separately and together.

J.Robledo-Moreno, G.Carleo, A.G. and J.Stokes, PNAS, 2022

Relative error as a function of hidden fermion number and depth of NN
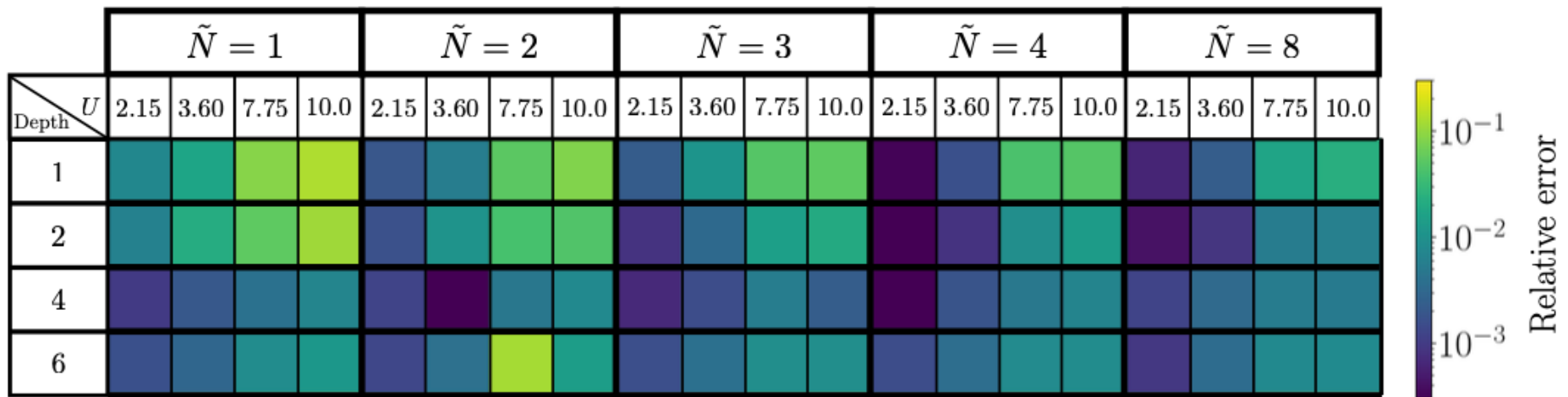## (4*4 Hubbard model at ½ filling)

Fig. 2. Effect of the number of hidden fermions and depth of the fully connected neural network that parametrizes the hidden sub-matrix in the expressive power of the hidden fermion determinant *ansatz*. The scale shows the relative error in the ground-state energy for different values of U given N_h and the neural network depth. The results correspond to the 4×4 Hubbard model at $n = 1/2$ filling.

J.Robledo-Moreno, G.Carleo, A.G. and J.Stokes, PNAS, 2022

NN-HFDS: Stripe order in the Hubbard model at 1/8 doping on 4*L cylinders (up to L=16)
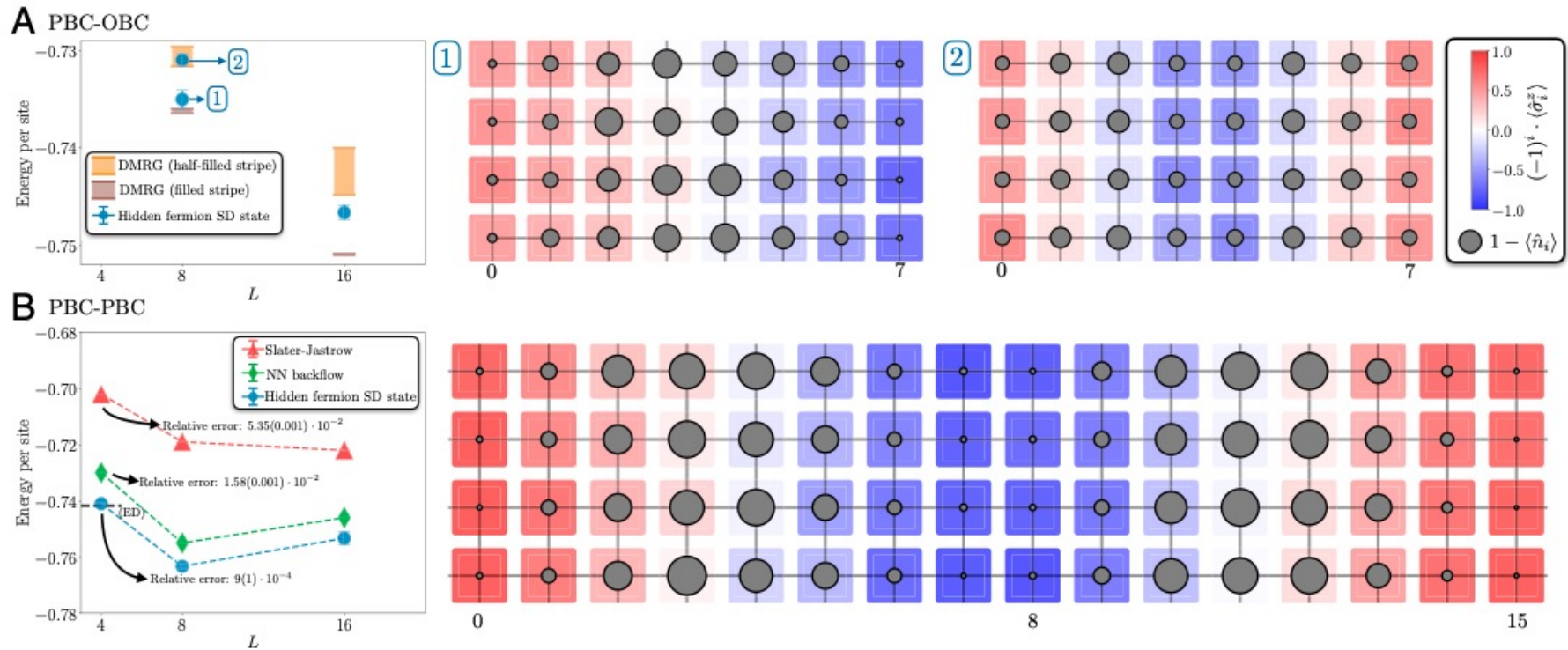

Fig. 4. Energy per site and competing charge and spin orders in the $4 \times L$ rectangular lattice at 1/8 hole doping ($n = 0.875$) and $U = 8$. (A) Periodic boundary conditions on the short side of the cylinder and open on the long side (PBC-OBC). *Left* panel compares the hidden-fermion determinant-state energies with DMRG energies. The width of the DMRG symbols shows the range of converged variational energies for different bond dimensions used in ref. 48. For $L = 8$, blue points labeled as 1 and 2 correspond to filled and half-filled stripes. *Right* panel shows the hole and staggered spin distribution for both metastable configurations. The diameter of the gray circles is proportional to the hole density. (B) Periodic boundary conditions along both sides of the rectangles (PBC-PBC). *Left* panel compares the hidden-fermion determinant-state energies with the Slater–Jastrow and neural-network backflow ansätze (from ref. 9). The dashed horizontal line marks the ED (4×4 with PBCs from ref. 51) energy. In the 4×4 lattice the relative error in the ground-state energy is displayed for each ansatz. *Right* panel shows the hole and staggered spin distributions in the 4×16 lattice.

J.Robledo-Moreno, G.Carleo, A.G. and J.Stokes, PNAS, 2022

Today's menu (cont'd):

- Fundamentals of Density Functional Theory, in a nutshell

- Teaching a neural network to implement the Hohenberg-Kohn correspondence

- Constructing Density Functionals using Machine Learning

- Some Applications

- Disclaimer: this is only an incomplete overview of an emerging and burgeoning field... basically to make you want to read/learn more about it.

Density Functional Theory in a Nutshell

$$\hat{H} = \hat{K} + \hat{V} + \hat{H}_{\mathrm{int}}$$

ab initio Hamiltonian for materials or molecules:

$$\hat{K} = -\frac{1}{2}\sum_{i=1}^{N}\nabla_{r_i}^2$$

$$\hat{V} = \sum_{i=1}^{N} v_n(r_i) = -\sum_{i=1}^{N}\sum_{n=1}^{N_n}\frac{Z_n}{|r_i - R_n|}$$

$$\hat{H}_{\mathrm{int}} = \frac{1}{2}\sum_{i\neq j=1}^{N}\frac{1}{|r_i - r_j|}$$
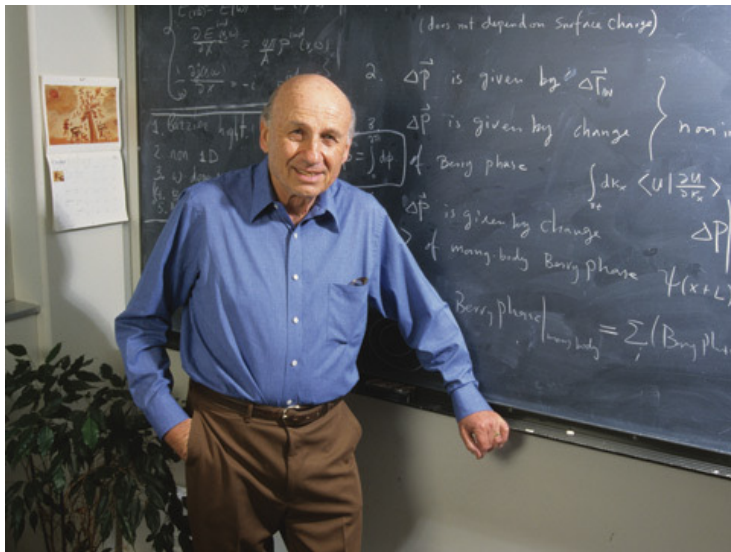
Or lattice model, e.g.:

$$\hat{K} = -t\sum_{\langle lm\rangle}(c_l^+ c_m + \mathrm{h.c.}) \;,\;\; \hat{V} = \sum_{l=1}^{L} v_l c_l^+ c_l \;,\;\; \hat{H}_{\mathrm{int}} = U\sum_{l=1}^{L}\hat{n}_l\hat{n}_{l+1}$$

Walter Kohn
Nobel Lecture, 1999

I begin with a provocative statement. *In general the many-electron wavefunction* $\Psi(r_1,...,r_N)$ *for a system of N electrons is not a legitimate scientific concept, when* $N \geq N_0$, *where* $N_0 \approx 10^3$.

Walter Kohn, Pierre Hohenberg and Lu Sham

Introduction to DFT: Useful References

- Julien Toulouse, *Introduction to DFT* lecture notes

- Kieron Burke and John Kozlowski *Lies my teacher told me about DFT* arXiv:2108.11534 and D.J.Carrascal et al. J.Phys:Cond Mat 29, 019501 (2017)

- N.Argaman and G.Makov *DFT: An Introduction* Am J.Phys 68, 69 (2000)

- R.O.Jones and O.Gunnarsson *The DFT formalism, its application and prospects* Rev Mod Phys 61, 689 (1989)

- Richard Martin *Electronic Structure* Cambridge University Press

Centerstage in DFT: The Local Density

$$n(r) = \langle \Psi_0 | \sum_{i=1}^{N} \delta(r - r_i) | \Psi_0 \rangle = \sum_{\sigma} \langle \Psi_0 | \psi_\sigma^+(r) \psi_\sigma(r) | \Psi_0 \rangle$$
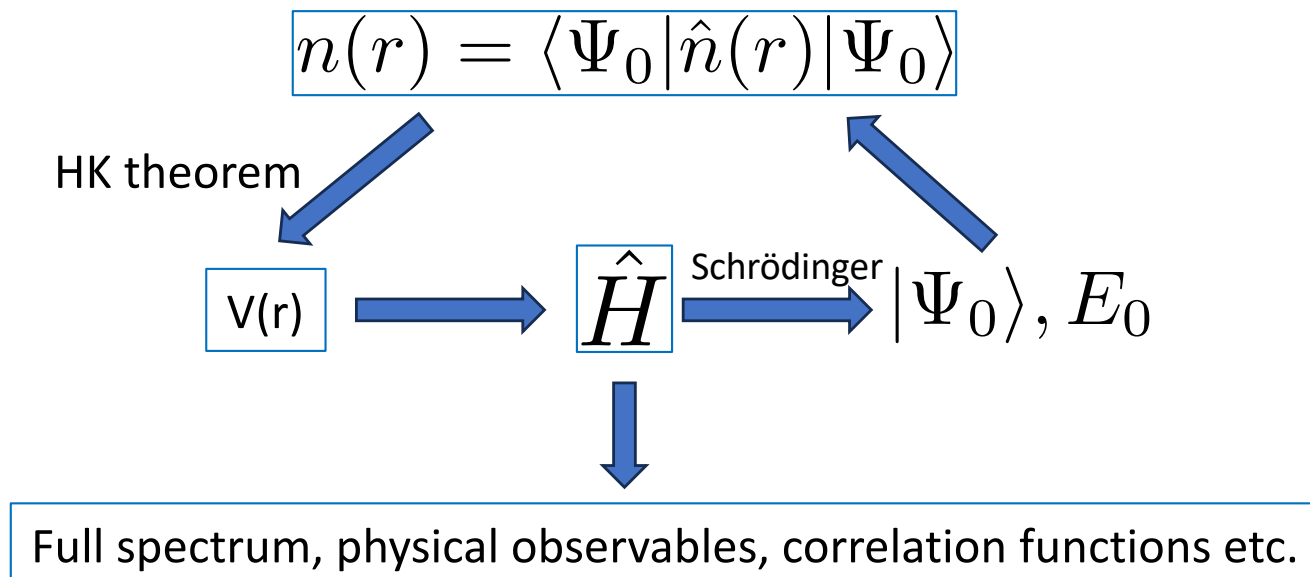
$$n(r) = N \int dr_2 \int dr_N \left| \Psi_0(r, r_2, \cdots, r_N) \right|^2 \ , \ \int dr \, n(r) = N$$

Lattice models:

$$n_l = \langle \hat{n}_l \rangle = \langle c_l^+ c_l \rangle \ , \ \sum_{l} n_l = N$$

Density Functional Theory – In a Nutshell (I)
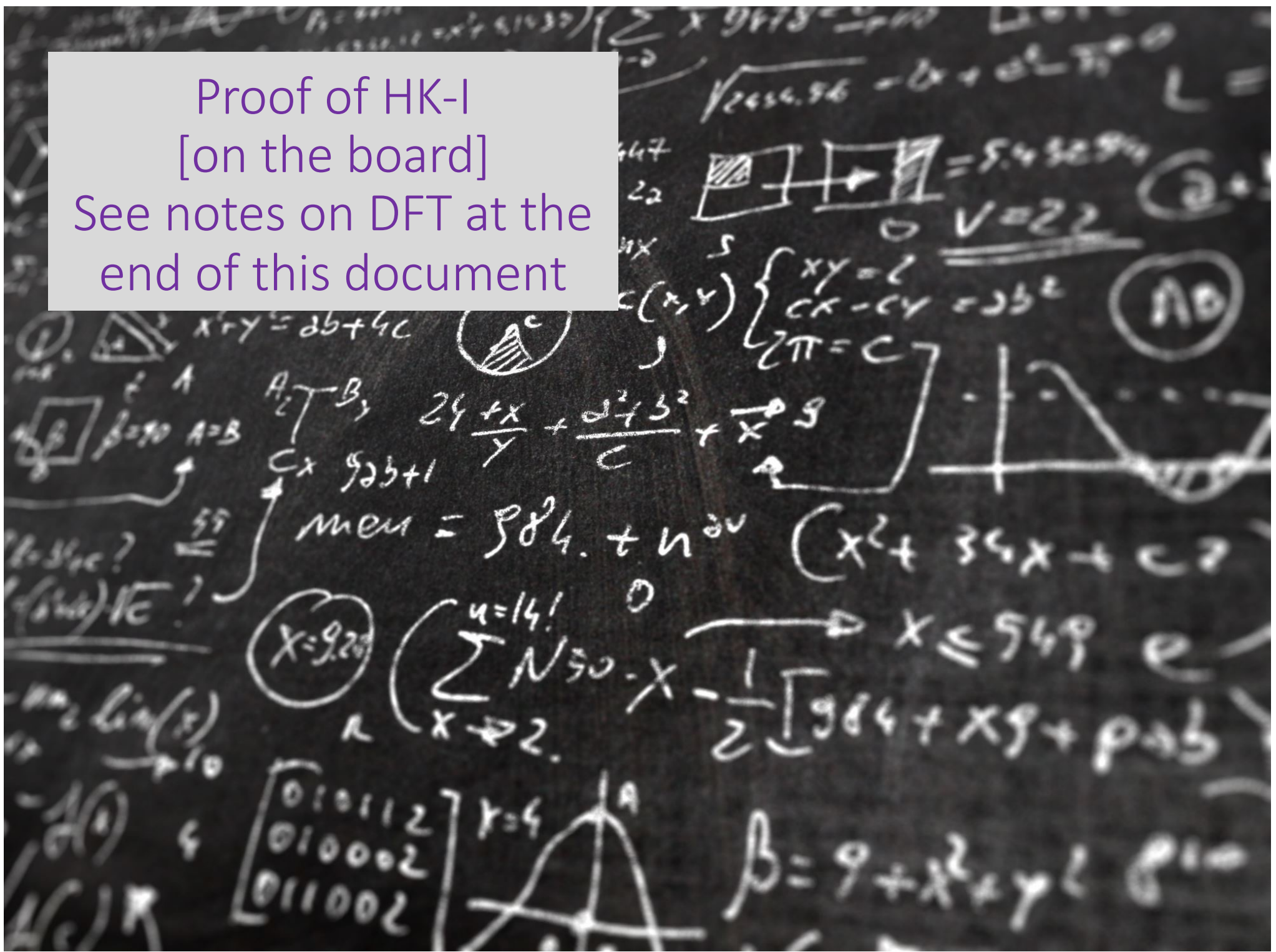
- Hohenberg-Kohn theorem I (1964):

- *The local charge density n(r) is in bijective correspondence with the one-body potential*

- *n(r) thus fully determines the Hamiltonian itself, and hence the full spectrum, etc.!* …. in principle.

$$n(r) = \langle \Psi_0 | \hat{n}(r) | \Psi_0 \rangle$$

HK theorem

V(r) $\longrightarrow$ $\hat{H}$ $\xrightarrow{\text{Schrödinger}}$ $|\Psi_0\rangle, E_0$

Full spectrum, physical observables, correlation functions etc.

Proof of HK-I
[on the board]
See notes on DFT at the
end of this document

Teaching a neural network to learn the HK map

Deep Learning the Hohenberg-Kohn Maps of Density Functional Theory

Javier Robledo Moreno[1,2,*] Giuseppe Carleo[1,†] and Antoine Georges[1,3,4,5,‡]

[1]*Center for Computational Quantum Physics, Flatiron Institute, New York, New York 10010, USA*
[2]*Center for Quantum Phenomena, Department of Physics, New York University, 726 Broadway, New York, New York 10003, USA*
[3]*Collège de France, 11 place Marcelin Berthelot, 75005 Paris, France*
[4]*CPHT, CNRS, École Polytechnique, IP Paris, F-91128 Palaiseau, France*
[5]*DQMP, Université de Genève, 24 quai Ernest Ansermet, CH-1211 Genève, Suisse*

A striking consequence of the Hohenberg-Kohn theorem of density functional theory is the existence of a bijection between the local density and the ground-state many-body wave function. Here we study the problem of constructing approximations to the Hohenberg-Kohn map using a statistical learning approach. Using supervised deep learning with synthetic data, we show that this map can be accurately constructed for a chain of one-dimensional interacting spinless fermions in different phases of this model including the charge ordered Mott insulator and metallic phases and the critical point separating them. However, we also find that the learning is less effective across quantum phase transitions, suggesting an intrinsic difficulty in efficiently learning nonsmooth functional relations. We further study the problem of directly reconstructing complex observables from simple local density measurements, proposing a scheme amenable to statistical learning from experimental data.
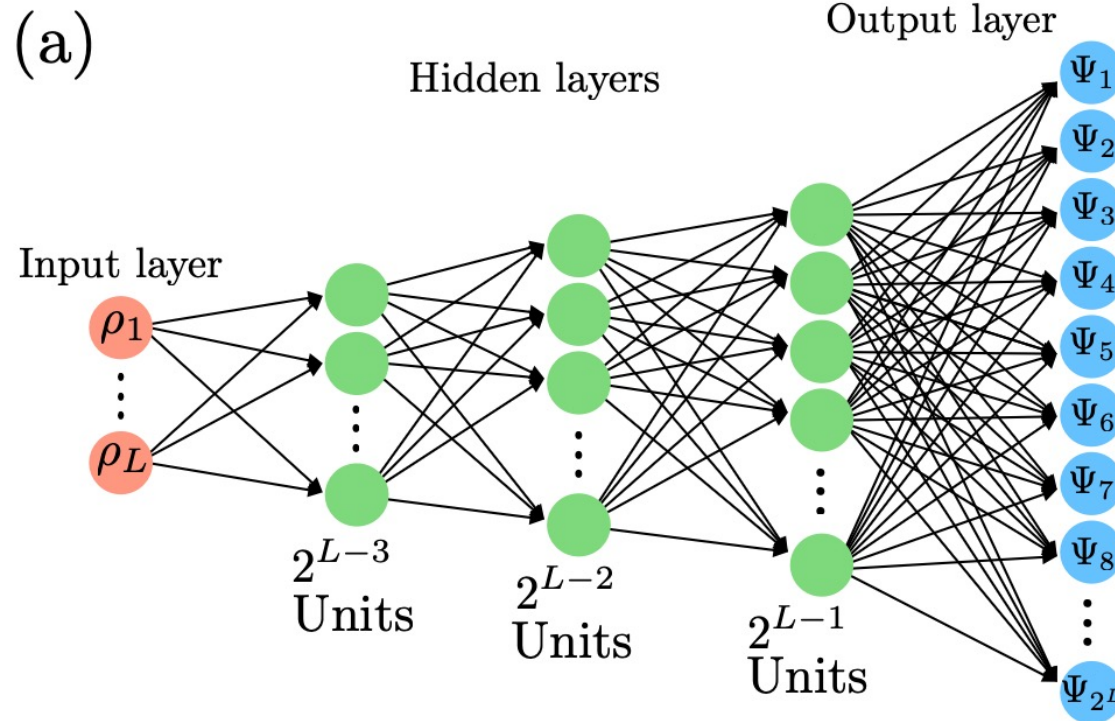
Implemented for a Toy Model:

Spinless fermions in d=1 with n.n. repulsion, half-filling (N=L/2)

$$\hat{H} = -t\sum_{l=1}^{L}(c_l^+ c_{l+1} + \text{h.c.}) + \sum_{l=1}^{L} v_l\, c_l^+ c_l + U\sum_{l=1}^{L}(\hat{n}_l - 1/2)(\hat{n}_{l+1} - 1/2)$$

- This model has a well-known phase diagram:

- U/t < 2: Metallic phase (`Luttinger liquid')
- U/t>2: Mott insulating phase with charge-density wave order, wavelength 2a
- The quantum critical point is in the Kosterlitz-Thouless universality class

- cf. e.g T. Giamarchi's book `Quantum Physics in One Dimension'

Network architecture (deep feedforward)

(a)

Output layer

Hidden layers

Input layer

ρ_1

ρ_L

2^{L-3} Units

2^{L-2} Units

2^{L-1} Units

Ψ_1
Ψ_2
Ψ_3
Ψ_4
Ψ_5
Ψ_6
Ψ_7
Ψ_8
Ψ_{2^L}

- Input layer: local density on each site
- Green neurons: ReLu activation
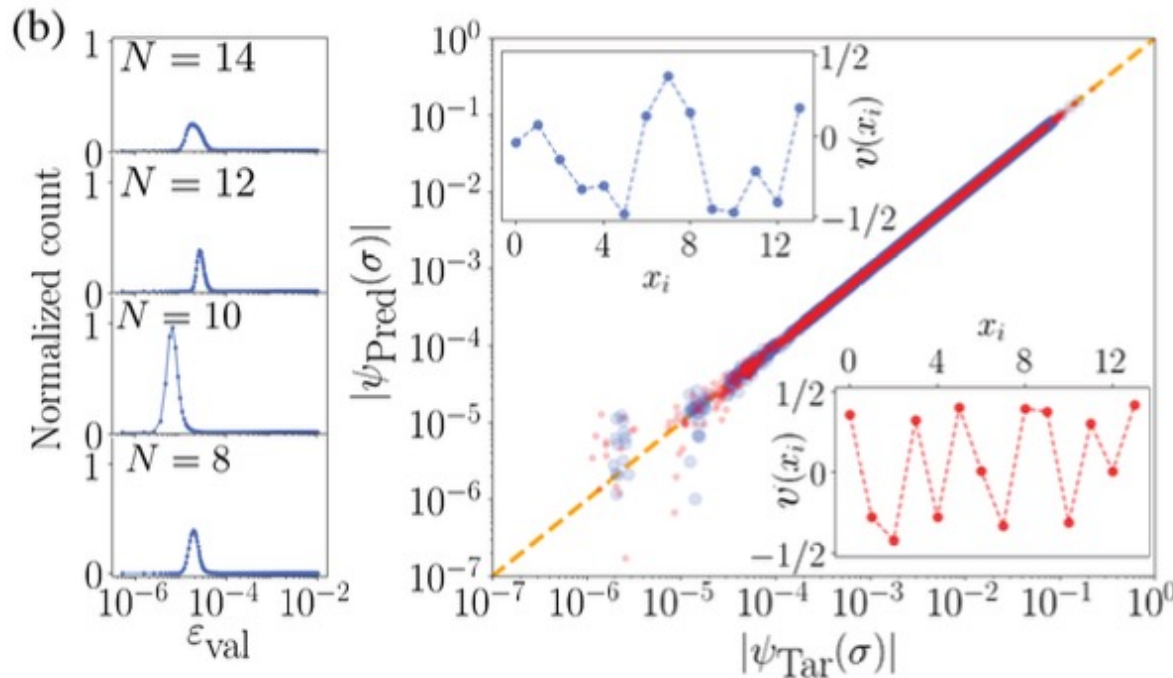- Output layer: 2^L components of wave-function, also insuring normalization

Training on random potentials with exact diagonalization

Cost function: Infidelity $\mathcal{L}_{\text{train}}(\{\theta\}) = 1 - |\langle\psi_{\text{tar}}|\psi_{\text{pred}}(\{\theta\})\rangle|,$

Training set in both phases: U/t=1 (LL), U/t=4 (MI/CDW) and U/t=2 (QCP)
Test on validation set (also generated by ED on unseen random potentials)
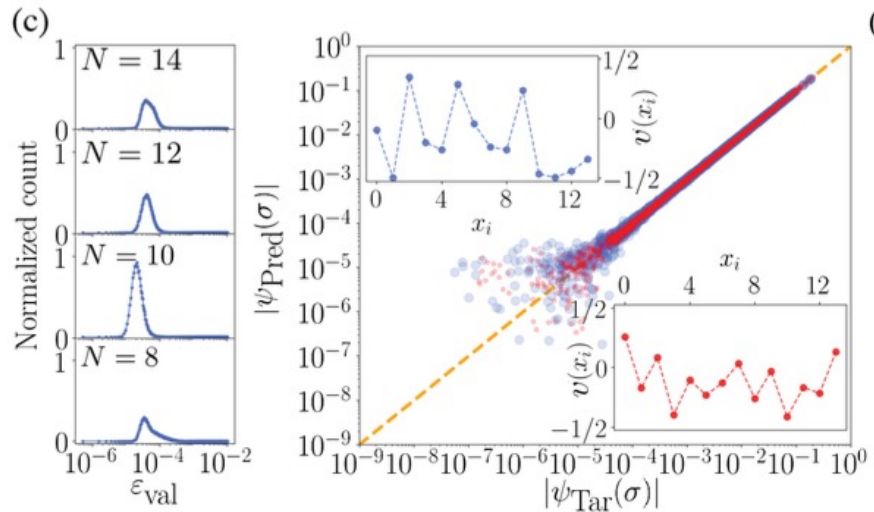
Histogram of errors (infidelity) on validation set

Testing the reconstruction of the wave-function for two random potentials (insets)

Metallic (LL) phase U/t=1

Mott Phase and Quantum Critical Point

Reconstruction also works well at the QCP U/t=2

Also in the Mott phase U/t=4
(although slightly larger errors):

We also found that the charge density
itself and the ground-state energy are
well reconstructed on the validation set

J. Robledo-Moreno, G. Carleo and A.G. PRL 125, 076402 (2020)
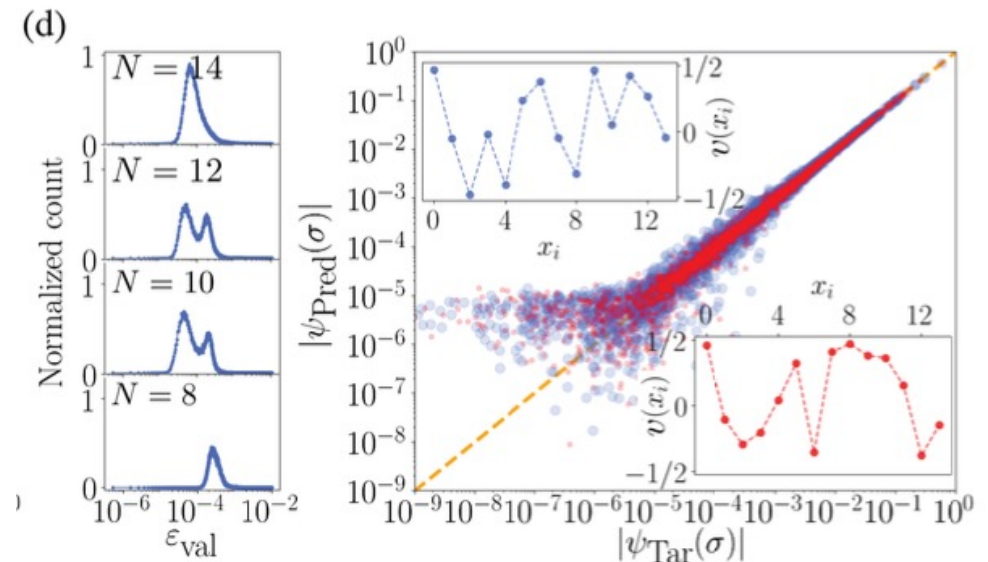
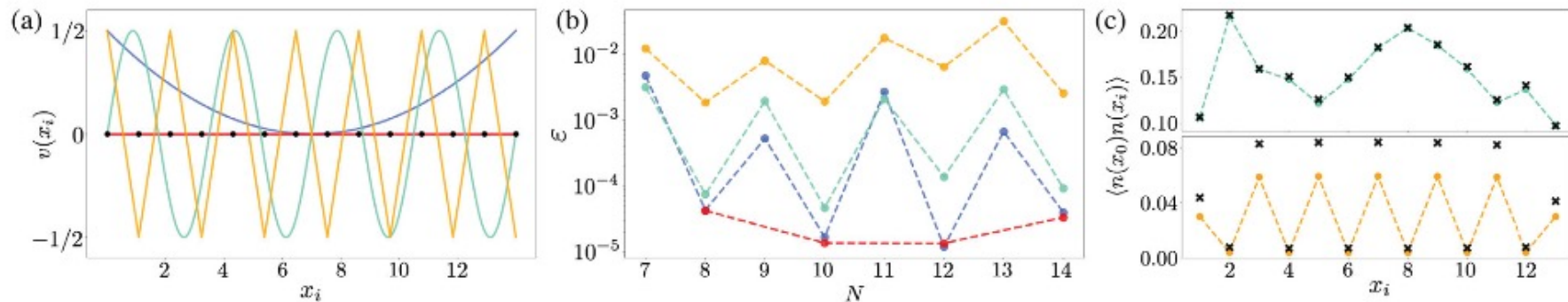# Test on structured (non-random) potentials at the QCP U/t=2

FIG. 2. Performance of the network in structured potentials. (a) Sketch of the tested potentials in a lattice with $N = 14$ sites. Potentials are quadratic (blue), no potential^{rma} (red), periodic with period $N/4$ (green), and staggered (orange). Black dots represent the position of the lattice sites. Panels (b) and (c) follow the same color code. (b) Error as defined in Eq. (4), as a function of the system size, when predicting the ground-state wave function given the potentials in panel (a). (c) Two-point density correlation functions computed from exact (dots connect by dashed lines) and ML-predicted (black crosses) wave functions. Only results for an even number of lattice sites are shown in this case as the ground state with an odd number of sites is degenerate.

The NN performs well, EXCEPT for a staggered potential (with periodicity 2a)
This may be rationalized: the system is unstable to a CDW with this periodicity
at the QCP and responds with an order parameter which depends on the
potential in a singular manner: the density functional is not smooth!

J. Robledo-Moreno, G. Carleo and A.G. PRL 125, 076402 (2020)

Direct reconstruction of correlation functions from the local density
(Note: the wave-function reconstruction is not directly scalable)

Grounded in the injective Hohenberg-Kohn map:

$$n(r) \rightarrow \text{Observables} \quad e.g. \quad C(r, r') = \langle \hat{n}(r) \hat{n}(r') \rangle$$
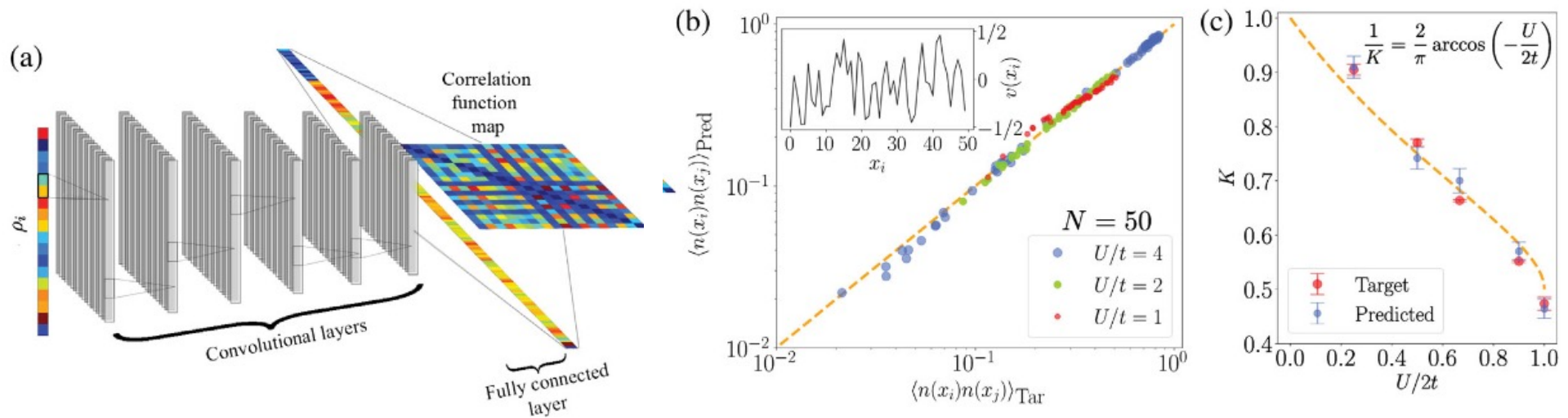
Training using DMRG with L=50

Reconstruction using a CNN is precise enough to allow for the determination of the Luttinger liquid parameter!

$$\langle n(x_i) n(x_{i+l}) \rangle \sim \frac{C_1}{l^2} + \frac{C_2 (-1)^l}{l^{2K}},$$

$$1/K = (2/\pi) \arccos(-U/2t)$$

J. Robledo-Moreno, G. Carleo and A.G. PRL 125, 076402 (2020)

DFT in a nutshell (II): Universal Density Functional and Total Energy Functional

Universal functional:

$$F[n(r)] \equiv \langle \Psi_0[n(r)] | \hat{K} + \hat{H}_{\mathrm{int}} | \Psi_0[n(r)] \rangle$$

$$E_{\mathrm{DFT}}[n(r)] = F[n(r)] + \int dr\, v(r) n(r)$$

$$E_0 = \mathrm{Min}_{n(r) \in \mathcal{D}_v} E[n(r)]$$

Hohenberg-Kohn II

Note (Levy, Lieb):

$$F[n] = \mathrm{Min}_{\Psi; \Psi \to n(r)} \langle \Psi | \hat{K} + \hat{H}_{\mathrm{int}} | \Psi \rangle$$

In essence, the whole construction is a Legendre transform!

Density Functional Theory in a Nutshell (II)

DFT in a nutshell (III): The Kohn-Sham Method
Derived here following a coupling-constant integration method

$$\hat{H}_\alpha = \hat{K} + \hat{V}_\alpha + \alpha \hat{H}_{\text{int}}$$

$$\forall \alpha \ , \ \langle \Psi_0^\alpha | \hat{n}(r) | \Psi_0^\alpha \rangle = n(r) \Rightarrow v(r) = v_\alpha[r; n(r)]$$

α=0: Kohn-Sham representative system

$$\left[\hat{k} + \hat{v}_{\text{KS}}\right] |\phi_a\rangle = \varepsilon_a |\phi_a\rangle \qquad n(r) = \sum_{j=1}^{N} |\phi_j(r)|^2$$

$$E_0[n(r)] = K_0[n(r)] + \int dr \, v_{\text{KS}}(r) n(r)$$

$$K_0[n(r)] = \sum_{i=1}^{N} \langle \phi_i | \hat{k} | \phi_i \rangle = \sum_{i=1}^{N} \varepsilon_i - \int dr \, v_{\text{KS}}(r) n(r)$$

DFT in a nutshell (III): The Kohn-Sham Method

Derived here following a coupling-constant integration method

$$E[n(r)] \equiv E_{\alpha=1}[n(r)] = E_0[n(r)] + \int_0^1 d\alpha \, \frac{\partial}{\partial\alpha} \langle \Psi_0^\alpha | \hat{H}_\alpha | \Psi_0^\alpha \rangle$$

$$\frac{\partial}{\partial\alpha} \langle \Psi_0^\alpha | \hat{H}_\alpha | \Psi_0^\alpha \rangle = \langle \Psi_0^\alpha | \frac{\partial \hat{H}_\alpha}{\partial\alpha} | \Psi_0^\alpha \rangle = \langle \Psi_0^\alpha | \frac{\partial \hat{V}_\alpha}{\partial\alpha} | \Psi_0^\alpha \rangle + \langle \Psi_0^\alpha | \hat{H}_{\text{int}} | \Psi_0^\alpha \rangle$$

$$\boxed{E[n(r)] = K_0[n(r)] + \int dr \, v(r) n(r) + \int_0^1 d\alpha \, \langle \Psi_0^\alpha | \hat{H}_{\text{int}} | \Psi_0^\alpha \rangle}$$

$$\boxed{E[n(r)] = K_0[n(r)] + \int dr \, v(r) n(r) + E_H[n(r)] + E_{\text{xc}}[n(r)]}$$

$$E_H[n(r)] == \frac{1}{2} \int dr dr' \, n(r) \, V_{\text{int}}(r - r') \, n(r') \qquad \text{Hartree}$$

$$E_{\text{xc}}[n(r)] == \frac{1}{2} \int dr dr' \, V_{\text{int}}(r - r') \int_0^1 d\alpha \, C_\alpha[r, r'; n] \qquad \text{Exchange-Correlation: the tough part!}$$

Machine Learning the gaps of semiconductors from the electron density

J. Robledo-Moreno, J. Flick and A.G. Phys Rev Materials 5, 083802 (2021)

Again grounded in HK-I: the full spectrum (and hence the gap) is in principle entirely determined by the charge density!

Remember: the KS gap is NOT the physical gap! We use DFT here *only* to compute n(r)

Train (and validate) on experimental gaps from a curated database of the experimental gaps for 472 materials (note: quite small number!)

P. Borlido et al. J. Chem. Theor. Comput. 15, 5069 (2019)

Used in that paper for benchmarking exchange-correlation functionals.
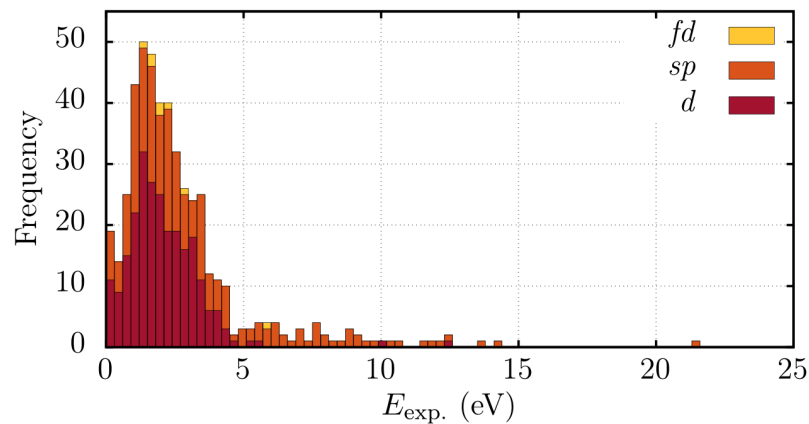

Figure 2. Histogram of experimental gaps in the data set. Boxes have a width of 0.3 eV. Colors represent the amount of each data set in the corresponding box. Description of the partial data sets is done in the main text.
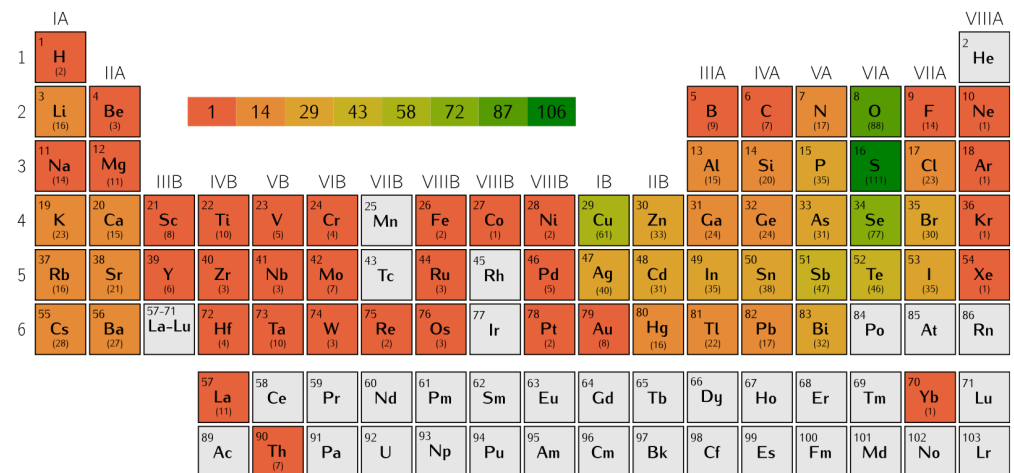

Figure 1. Frequency of elements in our data set. Gray boxes indicate elements not present in the data set.

Procedure:

- Input: charge density – represented by appropriate descriptors (see below)

- Charge density is calculated with an *approximate* density functional such as PBE (+van der Waals D2 correction)

- Output: bandgap

- Network is trained on a subset of the database (training set), validation on the rest of the dataset.

- Then, generalization/prediction

Charge density descriptors:

$$\rho^{\alpha\beta}(\vec{r} - \vec{R}^{\alpha\beta}) \approx \sum_{\substack{0 \leqslant n \leqslant n_{max} \\ 0 \leqslant l \leqslant l_{max} \\ -l \leqslant m_l \leqslant l}} C^{\alpha\beta}_{n,l,m} P_n^{orth}(r) Y_{l,m}(\theta, \phi),$$

$$d^{\alpha\beta}_{n,l} = \sum_{m=-l}^{l} \left[c^{\alpha\beta}_{n,l,m} \right]^2.$$

Sum over m insures rotational invariance

Network architecture

J. Robledo-Moreno, J. Flick and A.G.
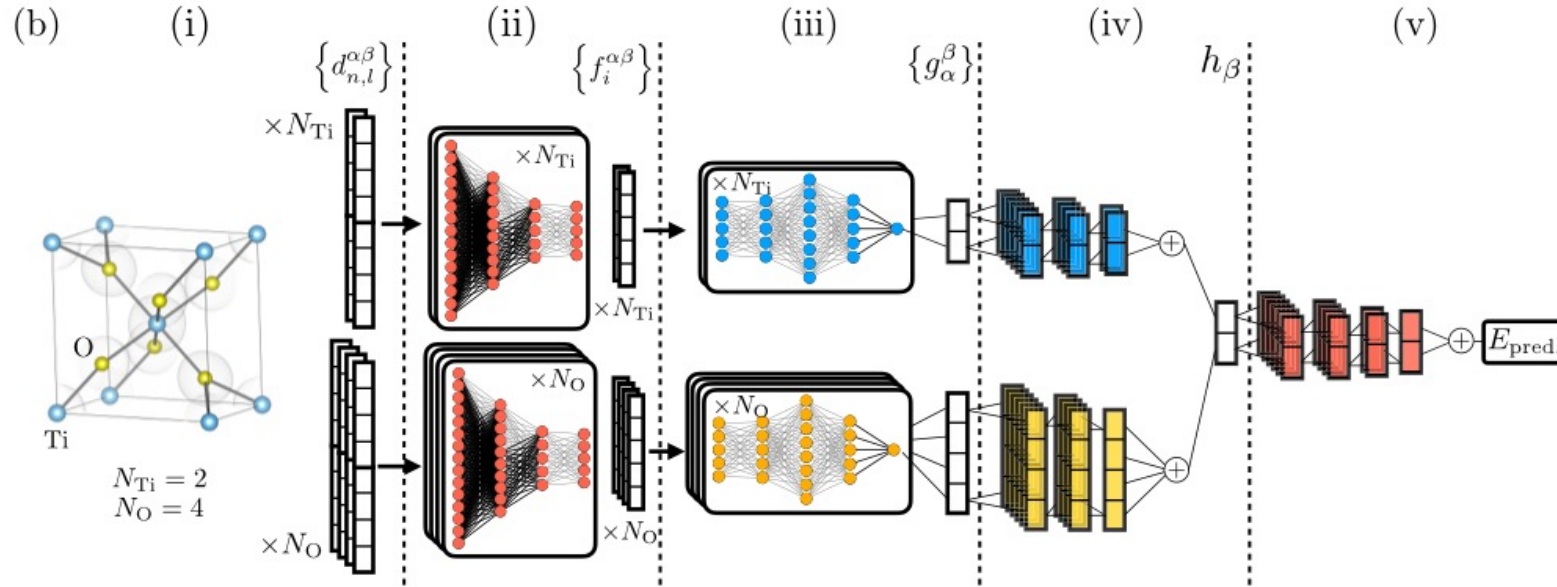Phys Rev Materials 5, 083802 (2021)

TABLE I. Detailed description of the modified Behler-Parrinello architecture and the intermediate data structures generated. See Fig. 1(b) for a schematic representation of the architecture and data structures. Bold symbols label trainable neural networks. In the data structures field, upper indices label the objects on a given set whereas lower indices label elements of an array.
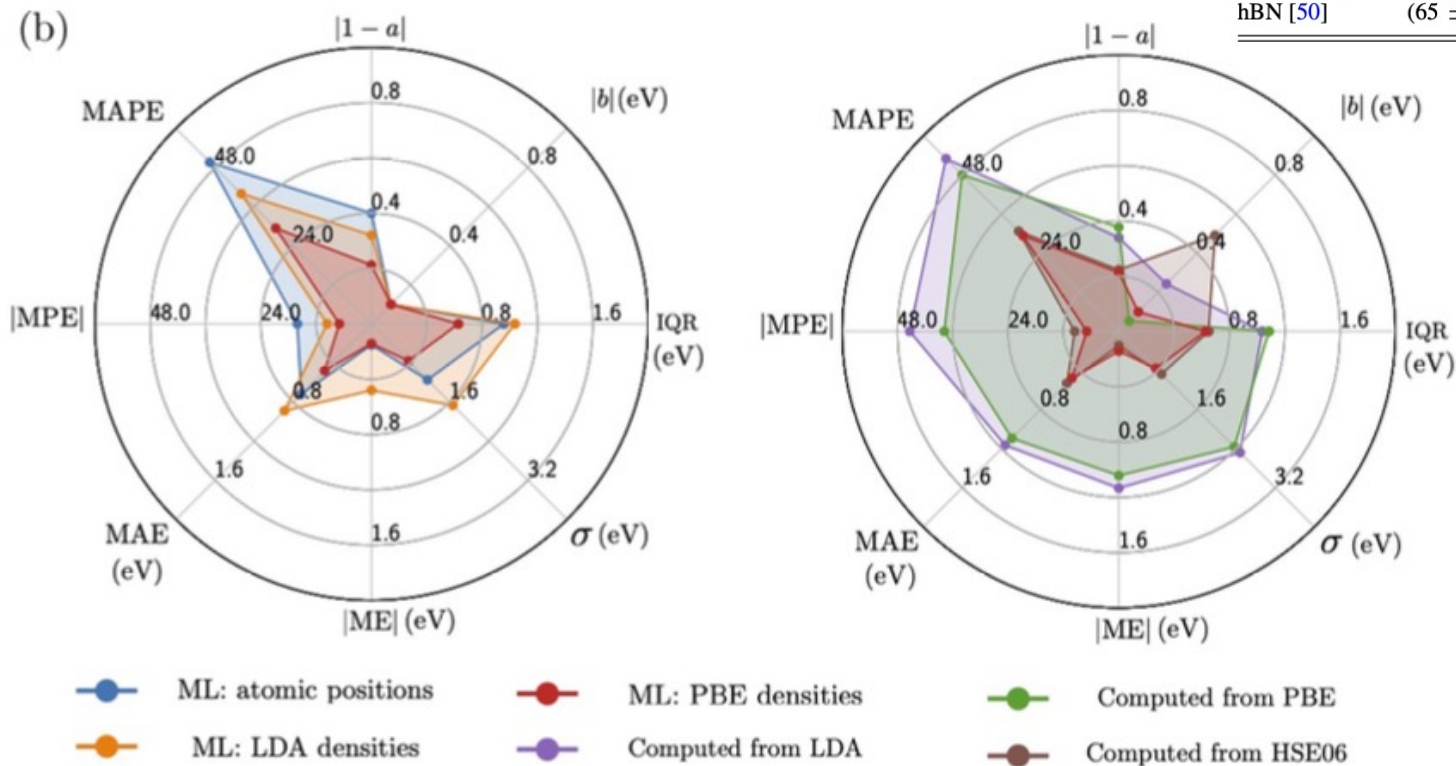
Name	Description
Operations:	
$PP(x)$	Preprocessing fully connected NN for feature extraction.
$BP^{\beta}(x)$	BP fully connected NN of atomic species β.
$DS^{\beta}(x)$	Deep Sets NN of atomic species β.
$DSsc(x)$	Deep Sets NN combining the output of each species block.
$\oplus^{\gamma}$	Concatenation across index γ.
Data structures:	
$\{d_{n,l}^{\alpha\beta}\}$	Rotationally invariant density descriptors; see Eq. (3).
$\{f_i^{\alpha\beta}\} = \{PP(d_{n,l}^{\alpha\beta})\}$	Preprocessed density features. $i = 1, \ldots, 5$.
$\{g_{\alpha}^{\beta}\} = \{\oplus^{\alpha}BP^{\beta}(f_i^{\alpha\beta})\}$	Output of the BP block concatenated for atoms in the same species.
$h_{\beta} = \oplus^{\beta}DS^{\beta}(g_{\alpha}^{\beta})$	Concatenation of the output of the species-specific Deep Sets across the different species.
$E_{\text{pred}} = DSsc(h_{\beta})$	Output of the Deep Sets species combiner. Predicted band gap.

Test set statistics

J. Robledo-Moreno, J. Flick and A.G.
Phys Rev Materials 5, 083802 (2021)

	ML from atomic positions	ML from LDA densities	ML from PBE densities
MoS$_2$ [48]	$(52 \pm 17)\%$	$(15 \pm 5)\%$	$(7 \pm 2)\%$
MoSe$_2$ [49]	$(44 \pm 15)\%$	$(40 \pm 12)\%$	$(15 \pm 5)\%$
hBN [50]	$(65 \pm 6)\%$	$(62 \pm 6)\%$	$(51 \pm 16)\%$

Legend:
- ML: atomic positions
- ML: LDA densities
- ML: PBE densities
- Computed from LDA
- Computed from PBE
- Computed from HSE06

- Left radar plot: ML from PBE densities (unsurprisingly) performs better than from LDA densities and, remarkably, *also better than learning directly from the atomic positions in the crystal structure!*
- Right radar plot: ML from PBE densities achieves comparable success than computation of gaps from computationally much more costly hybrid functional (HSE06)

Improving density functionals with ML

- Early work (*not* aimed at engineering a new DF but at *accelerating* DFT): J.Behler and M.Parrinello PRL 98, 146401 (2007)

- Early work: J.Snyder et al. PRL 108, 253002 (2012) Kernel regression on a model problem in d=1 – and several subsequent papers by Kieron Burke and collaborators such as Li et al. PRL 126, 036401 (2021) `KS equations as regularizer: building prior knowledge into ML physics'

- S.Dick and M.Fernandes-Serra Nature Comm. 11-3509 (2020) and PRB 104, L161109 (2021)

- M.Ma et al (Google Mountain View) Sci. Adv. 8, eabq0279 (2022) `Evolving symbolic density functionals'

- J.Kirkpatrick et al. (Google DeepMind) Science 374, 1385 (2021) [DM21 functional]

- R.Nagai, R.Akashi and O.Sugino npj Comp Mat (2020)

- H.Kurban et al. Sci Rep (2020) 12:14403

- *Many thanks to Matija Medvidović (Columbia/CCQ) and Javier Robledo-Moreno (NYU/CCQ) for discussions and guidance about this topic.*

The DeepMind21 Functional
J.Kirkpatrick et al. Science 374, 1385 (2021)
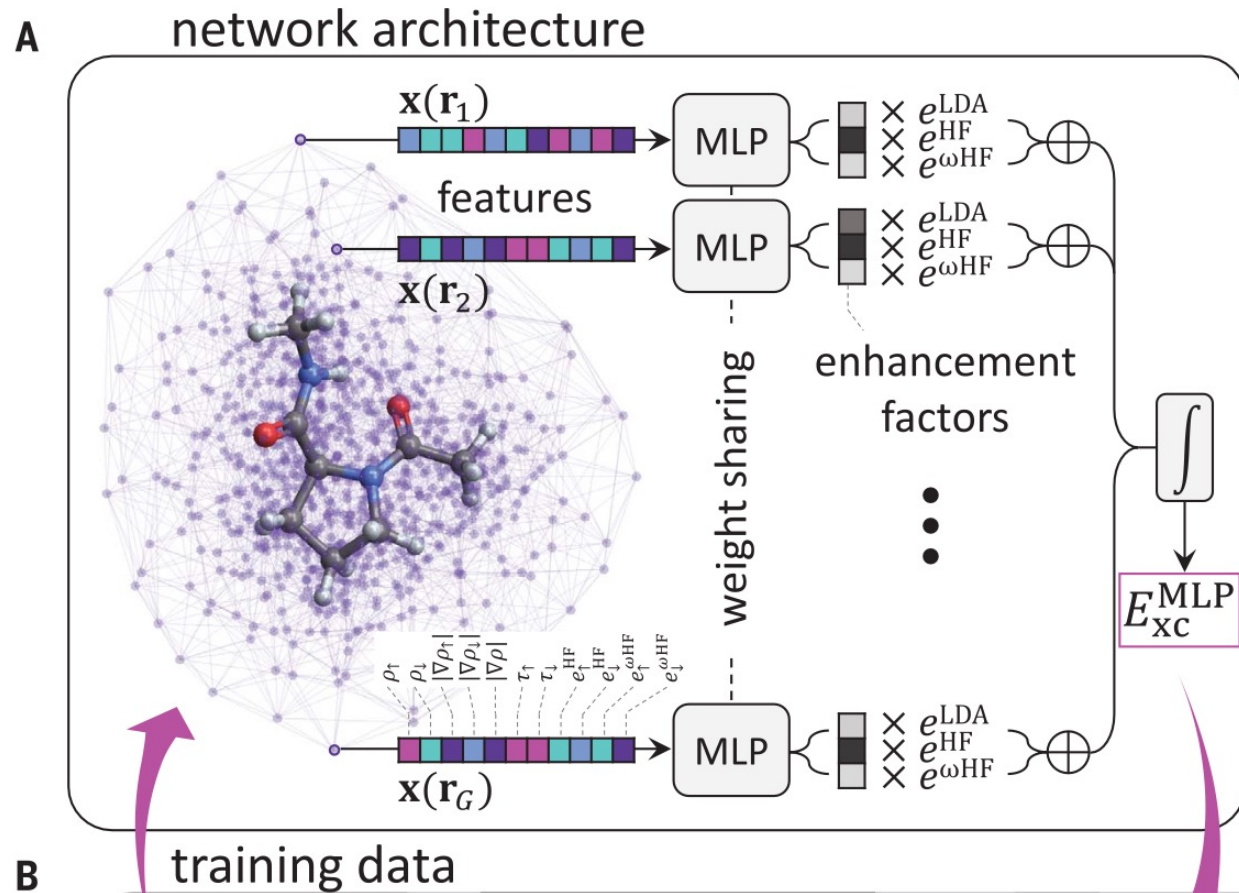
Strategy:
- `Features' from training dataset concatenated into vectors x(r)
- The x's are input to multilayer perceptrons
- Output is three weights f associated with the LDA exchange denergy density and two local versions of Hartree-Fock energy density

$$E_{xc}^{DM21} = E_{xc}^{MLP} + E_{vdW}^{D3BJ} \qquad \sim \text{`Local Hybrid'}$$

$$E_{xc}^{MLP}[n(r)] = \int dr \left[f_\theta^{LDA}[x(r)]e_x^{LDA}(r) + f_\theta^{HF}[x(r)]e^{HF}(r) + f_\theta^{\omega HF}[x(r)]e^{\omega HF}(r) \right]$$

Additionally the 3 exchange energies that are enhanced by our network are computed as $e^{\mathrm{LDA}}(\mathbf{r}) = -2\pi[(3/4\pi)(\rho^\uparrow + \rho^\downarrow)]^{4/3}$, $e^{\mathrm{HF}}(\mathbf{r}) = e_\uparrow^{\mathrm{HF}}(\mathbf{r}) + e_\downarrow^{\mathrm{HF}}(\mathbf{r})$, and $e^{\omega\mathrm{HF}}(\mathbf{r}) = e_\uparrow^{\omega\mathrm{HF}}(\mathbf{r}) + e_\downarrow^{\omega\mathrm{HF}}(\mathbf{r})$.

The 11 features, $\mathbf{x}(\mathbf{r})$, supplied at each grid point are computed from a (spin indexed $\sigma \in \{\uparrow, \downarrow\}$) density matrix Γ_{ab}^σ and basis set ψ_a as follows (using Einstein summation throughout):

- The density $\rho^\sigma(\mathbf{r}) = \Gamma_{ab}^\sigma \psi_a(\mathbf{r})\psi_b(\mathbf{r})$ in each spin channel.

- The square norm of the gradient of the density in each channel and of the total density $(|\nabla\rho^\uparrow|^2, |\nabla\rho^\downarrow|^2, |\nabla(\rho^\uparrow + \rho^\downarrow)|^2)$.

- The kinetic energy density $\tau^\sigma(\mathbf{r}) = \frac{1}{2}\Gamma_{ab}^\sigma[\nabla\psi_a(\mathbf{r}) \cdot \nabla\psi_b(\mathbf{r})]$ in each channel.

- The local HF features

$$e_\sigma^{\omega\mathrm{HF}}(\mathbf{r}) = -\frac{\Gamma_{ac}^\sigma \Gamma_{bd}^\sigma}{2} \int \psi_a(\mathbf{r})\psi_b(\mathbf{r}) \frac{\mathrm{erf}(\omega|\mathbf{r} - \mathbf{r}'|)}{|\mathbf{r} - \mathbf{r}'|} \psi_c(\mathbf{r}')\psi_d(\mathbf{r}') \, \mathrm{d}^3\mathbf{r}' \qquad (S3)$$

for both range-separated $\omega = 0.4$ and non-range-separated $\omega \to \infty$ in each spin channel. The single range-separated feature at $\omega = 0.4$ in atomic units was chosen empirically based on validation set performance.

J.Kirkpatrick et al. Science 374, 1385 (2021)
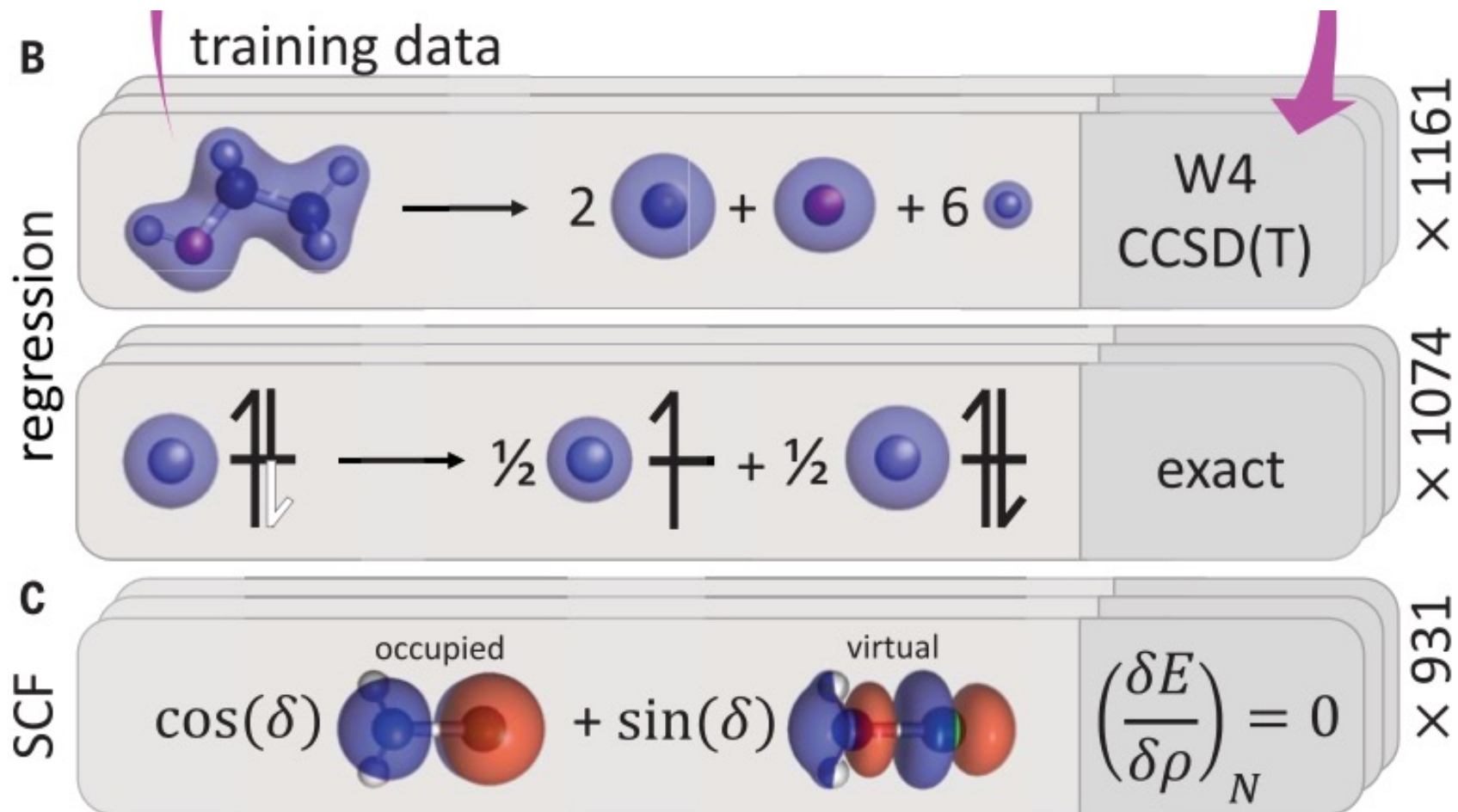
(B) The network is trained by using a dataset of KS input densities and high-accuracy energy labels for molecules and exact mathematical constraints.

(C) The gradient ofthe learned functional at fixed electron number (N) is supervised by requesting that the supplied orbitals are a stationary point of the total energy with respect to unitary rotation of occupied and virtual orbitals (illustrated by angle $\boldsymbol{\delta}$).
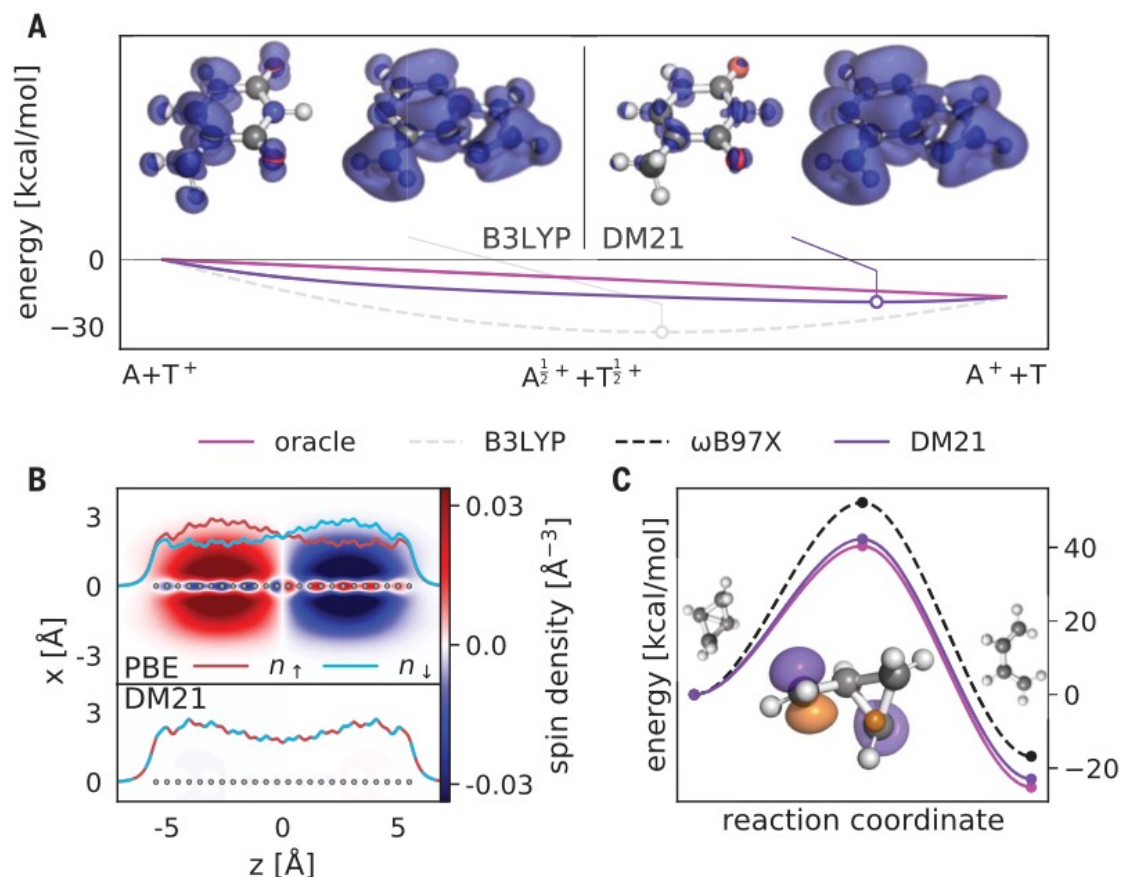
**Fig. 3. Exact constraints improve performance on challenging chemistry.** (**A**) Charge density for a singly ionized adenine-thymine base pair. B3LYP unphysically delocalizes charge on both base pairs despite adenine having a deeper ionization potential. Conversely, DM21 displays localization of charge on the adenine only. (**B**) Spin density for a compressed chain of 24 hydrogen atoms at 0.48 Å separation. The line density n for each spin channel is overlaid (supplementary materials, section 3.3). The PBE functional (41) breaks spin symmetry and leads to an apparent magnetization along the chain. This effect is also predicted by other functionals but is absent in DM21. (**C**) The conrotatory pathways of bicyclobutane isomerization. The HOMO of a single spin channel in an unrestricted calculation is shown for the transition states. Spin is delocalized across two atoms in the conrotatory path, requiring satisfaction of FS for accurate modeling. The oracle is diffusion Monte Carlo from (42).

J.Kirkpatrick et al. Science 374, 1385 (2021)

Fig. 4. State-of-the-art performance by DM21 on benchmarks. All errors are in kcal/mol. (**A**) The MoM error metric in each class of reactions from GMTKN55. More details are available in the supplementary materials, section 8.2. DM21 is compared with functionals at rungs two to five, with strong GMTKN55 metrics from (43): revPBE:D3$_{BJ}$ (44), SCAN:D3$_{BJ}$, and PW6B95:D3$_0$ (45). The dashed black line indicates the performance of the double-hybrid functional DSD-PBEP86:D3$_{BJ}$ (46). (**B**) Performance of DM21 compared with the SCAN functional and the three best performing hybrid functionals on three
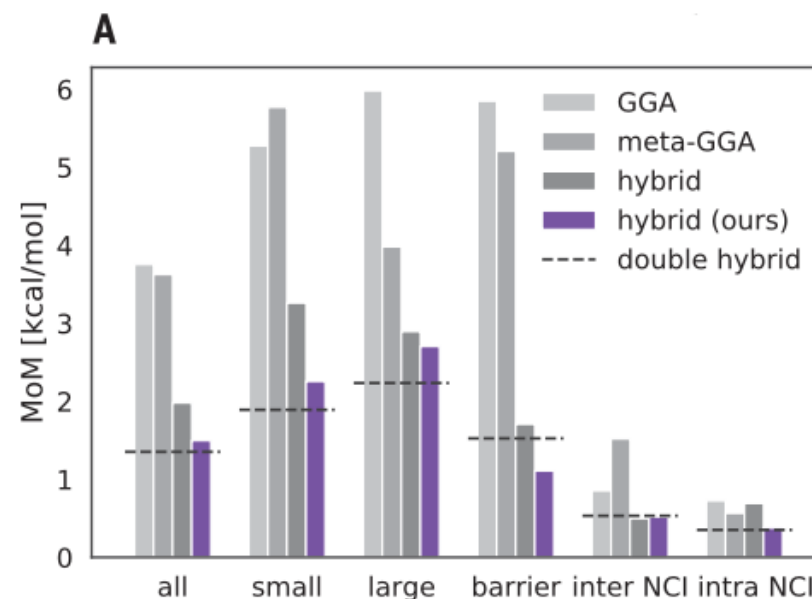
Notes on
Density Functional Theory

IX. INTRODUCTION TO DFT

Decompose the hamiltonian into kinetic energy, one-body (external) potential and inter-particle interactions:

$$\hat{H} = \hat{K} + \hat{V} + \hat{H}_{\text{int}} \tag{9.1}$$

In the context of electronic structure (fixed nuclei BO approximation, $e = \hbar = 1$), first quantized notation, $r_i = (\mathrm{r}_i, \sigma_i)$:

$$\hat{K} = -\tfrac{1}{2} \sum_{i=1}^{N} \nabla_{r_i}^2 \tag{9.2}$$

$$\hat{V} = \sum_{i=1}^{N} v_n(r_i) = -\sum_{i=1}^{N} \sum_{n=1}^{N_n} \frac{Z_n}{|r_i - R_n|} \tag{9.3}$$

$$\hat{H}_{\text{int}} = \tfrac{1}{2} \sum_{i \neq j=1}^{N} \frac{1}{|r_i - r_j|} \tag{9.4}$$

Or, for a lattice model of spinless electrons for example (with l, m lattice sites):

$$\hat{K} = -t \sum_{\langle lm \rangle} (c_l^+ c_m + \text{h.c.}) \ , \ \ \hat{V} = \sum_{l=1}^{L} v_l c_l^+ c_l \ , \ \ \hat{H}_{\text{int}} = U \sum_{l=1}^{L} \hat{n}_l \hat{n}_{l+1} \tag{9.5}$$

Local density:

$$n(r) = \langle \Psi_0 | \sum_{i=1}^{N} \delta(r - r_i) | \Psi_0 \rangle = \sum_{\sigma} \langle \Psi_0 | \psi_\sigma^+(r) \psi_\sigma(r) | \Psi_0 \rangle \tag{9.6}$$

or, in terms of the many-body wave-function:

$$n(r) = N \int dr_2 \int dr_N \left| \Psi_0(r, r_2, \cdots, r_N) \right|^2 \ , \ \int dr \, n(r) = N \tag{9.7}$$

For the lattice models:

$$n_l = \langle \hat{n}_l \rangle = \langle c_l^+ c_l \rangle \ , \ \sum_l n_l = N \tag{9.8}$$

A. The first Hohenberg-Kohn theorem (HK1)

Theorem: There is a bijective relation between the one-body potential $v(r)$ and the local charge density $v(r)$.

Proof. Ad absurdum. Assume that there are two different potentials $v_1 \neq v_2 + \text{const.}$, corresponding to the ground-state wave-functions $|\Psi_1\rangle$ and $|\Psi_2\rangle$ with the same charge density:

$$\langle \Psi_1 | \hat{n}(r) | \Psi_1 \rangle = \langle \Psi_2 | \hat{n}(r) | \Psi_2 \rangle = n(r) \tag{9.9}$$

First we show that $|\Psi_1\rangle \neq |\Psi_2\rangle$. Assume that they are the same. Then:

$$[K + V_1 + \hat{H}_{\text{int}}]|\Psi\rangle = E_1|\Psi\rangle \ , \ \ [K + V_2 + \hat{H}_{\text{int}}]|\Psi\rangle = E_2|\Psi\rangle \tag{9.10}$$

subtracting:

$$[V_1 - V_2]|\Psi\rangle = (E_1 - E_2)|\Psi\rangle \tag{9.11}$$

which implies:

$$\sum_{i=1}^{N} \Delta V(r_i)\, \Psi(r_1, \cdots, r_N) = \Delta E\, \Psi(r_1, \cdots, r_N) \tag{9.12}$$

which can only be satisfied if $\Delta V(r) = const.$. Hence $\Psi_1 \neq \Psi_2$. We can then apply the variational principle with a strict inequality:

$$E_1 = \langle \Psi_1 | \hat{H}_1 | \Psi_1 \rangle < \langle \Psi_2 | \hat{H}_1 | \Psi_2 \rangle = E_2 + \int dr\, [v_1(r) - v_2(r)] n(r) \tag{9.13}$$

Similarly we also obtain:

$$E_2 = \langle \Psi_2 | \hat{H}_2 | \Psi_2 \rangle < \langle \Psi_1 | \hat{H}_2 | \Psi_1 \rangle = E_1 + \int dr\, [v_2(r) - v_1(r)] n(r) \tag{9.14}$$

Adding these two equations, one obtains the contradiction:

$$E_1 + E_2 < E_2 + E_1 \tag{9.15}$$

Hence we must have that $v_1 = v_2 + const.$. QED

The proof is easily generalized to the lattice. The first part now reads:

$$\sum_l \Delta v_l \hat{n}_l \, |\Psi\rangle = \Delta E |\Psi\rangle \tag{9.16}$$

Decomposing the wavefunction over the occupation number basis, this yields:

$$\sum_n \psi(n) \sum_l \Delta v_l\, \delta_{n_l,1} |n\rangle = \Delta E \sum_n \psi(n) |n\rangle \tag{9.17}$$

which implies that for all n such that $\psi(n) \neq 0$, we must have:

$$\sum_l \Delta v_l\, \delta_{n_l,1} = \Delta E \tag{9.18}$$

which implies that $\Delta v_l = const.$ in which case (noting that $\sum_l \delta_{n_l,1} = N$ for any n in the canonical ensemble) one obtains: $\Delta E = N\Delta v$. The second part of the proof is unchanged.

Hence, remarkably, there is a unique potential and hence a unique Hamiltonian (given the form of K and H_{int}) corresponding to a given local density $n(r)$:

$$n(r) \to_{HK} v(r) \to_{def} \hat{H} \to_{S.Eq.} |\Psi_0\rangle \to n(r) = \langle \Psi_0 | \hat{n}(r) | \Psi_0 \rangle \tag{9.19}$$

This also implies that the local density uniquely defines (in principle...) the average value of any operator, or any correlation function:

$$n(r) \to \langle \hat{O} \rangle \;,\; C(r_1, \cdots, r_n; t_1, \cdots, t_n) \tag{9.20}$$

but this mapping is injective, not bijective.

B. Universal density functional and total energy functional

Denoting by $|\Psi_0[n(r)]\rangle$ the unique ground-state with local density $n(r)$, Hohenberg and Kohn define:

$$F[n(r)] \equiv \langle \Psi_0[n(r)] | \hat{K} + \hat{H}_{\text{int}} | \Psi_0[n(r)] \rangle \tag{9.21}$$

This is a *universal functional of the density*, which only depends on the form of the interaction term and kinetic energy, not on the potential (i.e on the specific material at hand).

The total energy functional, for a given potential (i.e. a given material) is now:

$$E_{\text{DFT}}[n(r)] = F[n(r)] + \int dr\, v(r)n(r) \tag{9.22}$$

The second HK theorem states that the ground-state energy is obtained by minimizing $E[n]$ over v-representable densities:

$$E_0 = \text{Min}_{n(r)\in\mathcal{D}_v}\, E[n(r)] \tag{9.23}$$

$F[n]$ can also be viewed (Levy, Lieb) as:

$$F[n] = \text{Min}_{\Psi;\Psi\to n(r)}\, \langle\Psi|\hat{K} + \hat{H}_{\text{int}}|\Psi\rangle \tag{9.24}$$

in which the minimization is over all many-particle wave-functions that yield the local density $n(r)$.

The whole construction can be viewed as a Legendre transform: we can view the energy as a functional of the external potential $v(r)$. The bijective map between $v(r)$ and $n(r)$ guarantees that we can Legendre transform this functional into the universal functional F (aka 'Gibbs' functional):

$$n(r) = \frac{\delta E[v(r)]}{\delta v(r)} \to F[n(r)] = E\left[v[n(r)]\right] - \int dr\, v[n(r)]n(r) \tag{9.25}$$

As usual with Legendre transforms, we have:

$$v(r) = -\frac{\delta F[n(r)]}{\delta n(r)} \tag{9.26}$$

which means that the equilibrium density of the system is the one that minimizes the functional $E_{\text{DFT}}[n(r)]$ defined above.

All the statements above are exact (with proper conditions on the density and potential), but rather formal: the expression of the density functional is unknown! Even the kinetic energy part of the functional is not straightforward to express in terms of $n(r)$ only - this is where the Kohn-Sham construction is crucial.

C. DFT: the Kohn-Sham method

I now introduce a cornerstone of DFT which is crucial to its practical implementation: the Kohn-Sham *representation* of the charge density by a non-interacting *reference system* - a Slater determinant of one-particle orbitals. It is important to note that this is only a representative system: these orbitals are not meant to describe the excitations of the physical system, nor is this Slater determinant supposed to be a good description of the many-body wave-function. For example, a Mott insulator may well have an *exact* Kohn-Sham system which is gapless! The gap of the Kohn-Sham spectrum should not be interpreted as the gap in the physical spectrum, even for weakly interacting systems.

I follow here a derivation based on coupling constant integration (not quite the mainstream derivation, but my favorite one). Consider the modified hamiltonian:

$$\hat{H}_\alpha = \hat{K} + \hat{V}_\alpha + \alpha\,\hat{H}_{\text{int}} \tag{9.27}$$

In this expression, $\hat{V}_\alpha$ is the unique α-dependent potential corresponding to a given charge density $n(r)$ (by virtue of the HK map, which applies to any α):

$$\forall \alpha \ , \ \langle \Psi_0^\alpha | \hat{n}(r) | \Psi_0^\alpha \rangle \ = \ n(r) \ \Rightarrow \ v(r) = v_\alpha[r; n(r)] \tag{9.28}$$

with Ψ_0^α is the ground-state of $\hat{H}_\alpha$.

Note that $\hat{H}_\alpha$ interpolates between the physical hamiltonian for $\alpha = 1$ with $v_1(r) = v(r)$ the potential of the material of interest, and a non-interacting hamiltonian in which the physical potential has been replaced by a different one, $v_0(r)$ which is such that it reproduces the physical density of the material in the (hypothetical) absence of interactions. This is the Kohn-Sham idea. The effective *Kohn-Sham potential* $v_0(r) \equiv v_{KS}(r)$ is the position-dependent Lagrange multiplier that we need to apply in the absence of interactions to reproduce the charge density of the physical system - it should not be confused with the physical potential $v(r)$.

The ground-state wave-function of $\hat{H}_0$ is a Slater determinant of single-particle orbitals, the *Kohn-Sham orbitals*:

$$\left[\hat{k} + \hat{v}_{KS} \right] | \phi_a \rangle = \varepsilon_a | \phi_a \rangle \tag{9.29}$$

($\hat{k}$ is the one-body kinetic energy operator). The density $n(r)$ is obtained as:

$$n(r) \ = \ \sum_{j=1}^{N} |\phi_j(r)|^2 \tag{9.30}$$

in which the sum is over the N lowest-energy occupied KS orbitals, the ground-state of $\hat{H}_0$ being the SD:

$$\Psi_0^{\alpha=0}(r_1, \cdots, r_N) \ = \ \det\left[\phi_j(r_i) \right] \tag{9.31}$$

To find the KS representation for a given $n(r)$, we can e.g. proceed iteratively: we solve the one-particle Schrödinger equation for an initial guess of the potential v_0, compute $n(r)$ and then update the potential until the target charge density is reached.

We now formally construct the density functional by coupling constant integration:

$$E[n(r)] \ \equiv \ E_{\alpha=1}[n(r)] \ = \ E_0[n(r)] \ + \ \int_0^1 d\alpha \, \frac{\partial}{\partial \alpha} \langle \Psi_0^\alpha | \hat{H}_\alpha | \Psi_0^\alpha \rangle \tag{9.32}$$

in which:

$$E_0[n(r)] = K_0[n(r)] + \int dr \, v_{KS}(r) n(r) \tag{9.33}$$

in which K_0 is the kinetic energy of electrons in the reference non-interacting (KS) system:

$$\boxed{K_0[n(r)] \ = \ \sum_{i=1}^{N} \langle \phi_i | \hat{k} | \phi_i \rangle \ = \ \sum_{i=1}^{N} \varepsilon_i - \int dr \, v_{KS}(r) n(r)} \tag{9.34}$$

It is a key advantage of the KS construction to provide an explicit construction of the kinetic term in the functional. Note however that K_0 is *not* the kinetic energy of electrons in the physical system.

Using the Hellmann-Feynman theorem:

$$\frac{\partial}{\partial \alpha} \langle \Psi_0^\alpha | \hat{H}_\alpha | \Psi_0^\alpha \rangle \ = \ \langle \Psi_0^\alpha | \frac{\partial \hat{H}_\alpha}{\partial \alpha} | \Psi_0^\alpha \rangle \ = \ \langle \Psi_0^\alpha | \frac{\partial \hat{V}_\alpha}{\partial \alpha} | \Psi_0^\alpha \rangle + \langle \Psi_0^\alpha | \hat{H}_{int} | \Psi_0^\alpha \rangle \tag{9.35}$$

The first term is readily integrated and we obtain:

$$E[n(r)] \;=\; K_0[n(r)] + \int dr\, v(r)n(r) \;+\; \int_0^1 d\alpha\, \langle \Psi_0^\alpha | \hat{H}_{\text{int}} | \Psi_0^\alpha \rangle \tag{9.36}$$

We have thus obtained a formal construction of the exact density functional! We can proceed a bit further and note that the average of the interaction term can be related to the connected density-density correlation function:

$$C_\alpha(r, r') \;\equiv\; \langle \Psi_0^\alpha | \left(\hat{n}(r) - n(r) \right) \left(\hat{n}(r') - n(r') \right) | \Psi_0^\alpha \rangle \tag{9.37}$$

This is the density-density correlator of a system with interactions modified by $\alpha \in [0,1]$ and constrained (through v_α) to have the specified density $n(r)$. This allows to pull out the Hartree term in the above expression and we finally obtain:

$$\boxed{E[n(r)] \;=\; K_0[n(r)] + \int dr\, v(r)n(r) \;+\; E_H[n(r)] \;+\; E_{\text{xc}}[n(r)]} \tag{9.38}$$

with:

$$\boxed{E_H[n(r)] \;==\; \frac{1}{2} \int dr dr'\, n(r)\, V_{\text{int}}(r - r')\, n(r')} \tag{9.39}$$

$$\boxed{E_{\text{xc}}[n(r)] \;==\; \frac{1}{2} \int dr dr'\, V_{\text{int}}(r - r') \int_0^1 d\alpha\, C_\alpha[r, r'; n]} \tag{9.40}$$

the Hartree and exchange-correlation functional, respectively.

Finding a satisfactory approximation to the exchange-correlation part of the functional is the central question for practical applications of DFT.

D. DFT-KS self-consistent loop

We now have all the elements in hand to outline the procedure for minimizing the density functional. We have to solve:

$$0 \;=\; \frac{\delta E}{\delta n(r)} \;=\; v(r) - v_{\text{KS}}(r) + v_H(r) + v_{\text{xc}} \tag{9.41}$$

in which we have used $K_0 = E_0 - \int dr v_{\text{KS}}(r)n(r)$, $\delta E_0 / \delta n(r) = 0$ and the Hartree and exchange-correlation potential are given by:

$$v_H(r) = \int dr\, V_{\text{int}}(r)n(r) \;\;,\;\; v_{\text{xc}}(r) \equiv \frac{\delta E_{\text{xc}}}{\delta n(r)} \tag{9.42}$$

To find the solution , one proceeds iteratively:

- Initialize density to $n(r)$

- Compute the Kohn-Sham potential for that density: $v_{\text{KS}}(r) = v(r) + v_H[r; n] + v_{\text{xc}}[r; n]$

- Solve the one-particle Schrödinger equation in the KS potential

- Compute again $n(r)$ from the new KS orbitals

- Repeat loop until convergence.

At the end of the self-consistency cycle, the total energy can be computed as:

$$E = \sum_i \varepsilon_i + \int dr \, [v(r) - v_{\text{KS}}(r)]n(r) + E_H + E_{xc} \tag{9.43}$$

$$= \sum_i \varepsilon_i - E_H + E_{xc} - \int dr \, v_{\text{xc}}(r)n(r) \tag{9.44}$$